Università degli Studi di Udine

Dottorato di Ricerca in
Tecnologie Chimiche ed Energetiche
Ciclo XXV

DESIGN AND OPTIMIZATION OF A GAS BURNER FOR TPV APPLICATION

Dott. Giulio CASSIO

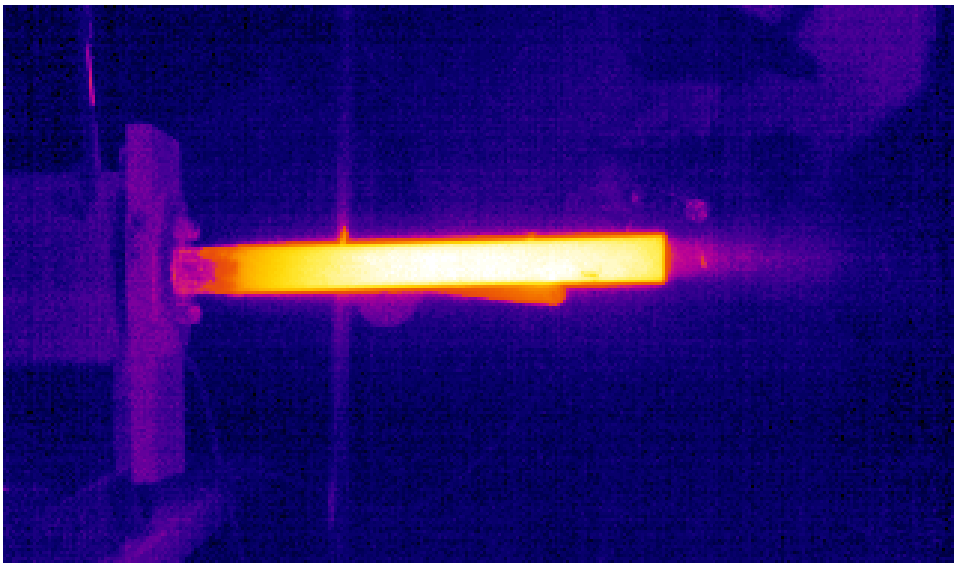

COMMISSIONE

Prof. Marco CAVAZZUTI	Revisore
	Revisore
Prof. Stefano DEL GIUDICE	Commissario
Prof. Giorgio PAVESI	Commissario
Prof. Fabrizio BEZZO	Commissario
Prof. Carlo POLONI	Supervisore
Prof. Alfredo SOLDATI	Coordinatore del Dottorato

Author's Web Page: www.ing.units.it

Author's e-mail: gcassio@units.it

Author's address:

Dipartimento di Ingegneria Meccanica e Navale
Università degli Studi di Trieste
Via Valerio, 10
34127 Trieste – Italia
tel. +39 040 558 3231
web: http://http://www.ing.units.it/

Contents

List of Figures

1

SYSTEM

A TPV system basically exploits cogeneration to enhance overall efficiency, this means both heat and electrical power are positive effects. In order to understand how a TPV system works and is designed, it is essential to divide it in fundamental parts and track energy fluxes, as shown in Fig. 1.1. This is only a brief description to understand the basics that overcome the device, then, in the next sections all these parts will be fully presented and analyzed:

1. Heat generator: produces the amount of thermal power needed to bring the radiator to incandescence. The generation of heat can be guaranteed in very different ways, including combustion, chemical reactions or solar concentration, for example.

2. Emitter: reaching high temperatures it generates electromagnetic radiation. Shape and dimensions depend on the system configuration, while chemical, physical and optical properties greatly influence spectral emissivity.

3. Thermophotovoltaic cells: cells receive radiation from the emitter and generate electric power. This is a critical part of the system, which has a significant weight on the overall performance.

4. Filters: these belong to the optical devices which can be used to optimize the coupling between emitter and cells. Filters are selective barriers which reflect non useful radiation back to the emitter.

5. Auxiliary systems: other devices supervise the cooling of the cell circuits, flow rate of air and gas and the operation of electronic equipment.

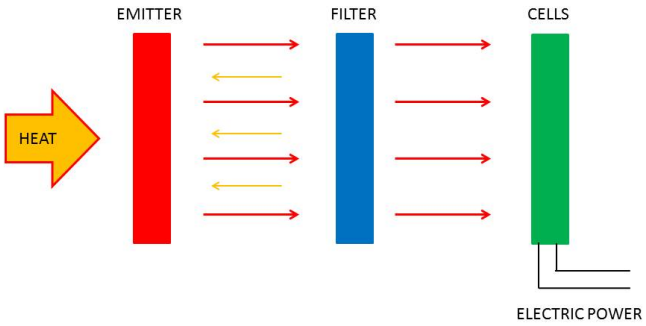

Figure 1.1: Energy flux of a TPV system

1.1 Heat generator

The heat generator is an essential part. It must guarantee the necessary power for heating up the emitter. Since a TPV system can have very different destinations and energy demands, different energy sources can be used. At the moment gas fired burners are frequently used, as in Refs. (1) and (2). But particular applications using solar energy or liquid fuels, as in Refs. (3) and (4), have also been studied. A very specific application of this kind of technology is for space missions, developed by NASA. In this case energy is provided by fuel cells working on radiative isotopes.

Although having many different configurations, the heat source must have determined characteristics. High energy density is preferred in order to minimize fuel consumption or increase operating time. Dimensions have to be limited, keeping low weight and size, especially for transportation purposes. Simplicity and reliability are also important considering maintainance costs. Noise has to minimized because the device is likely to be used not in an industrial environment. Most important of all, pollution production must be kept under control, beneath law constrictions. This limits operating conditions to temperatures below 1500 °C - 1600 °C in order not to enhance the production of NO_x.

If we consider all this issues and at the same time maximization of heat transfer to the emitter, it is easy to understand that designing and optimizing a burner for this particular device is not a simple task at all.

1.2 Emitter

The emitter, or radiator as can be called, converts thermal power produced by the heat source into radiation, having thus a great influence on the overall performances of the system. As said before the choices in the design of the emitter depend on the configuration of the whole system, but all are taken to maximize the emitted power. These cannot be treated in a general way and so will not be analyzed here. Despite this, two areas of interest must be considered in the design of the emitter:

- geometrical characteristics
- material properties

Geometrical characteristics are shape, dimensions and thickness of the material. These values are determined in order to have high and uniform temperatures on the surface.The choice of the material is a very important aspect for the emitter since, both mechanical, thermal and optical properties determine the emitted power. Mechanical properties regard especially resistance to high temperatures and frequent changes in loads. Only particular metallic or ceramic materials can resist up to temperatures exceeding 2000 °C, without melting or having mechanical fractures. Ceramic materials have very high melting temperatures but although very rigid, these are very fragile too, thus bringing an issue with the coupling with other parts of the TPV system.

Optical properties are probably the most important in the selection of the emitter material. Two aspects characterize the radiative power: emissivity and wavelength dependence. Emissivity is by definition the ability of a surface to emit energy by radiation, it is the ratio of energy radiated by a particular material to the energy radiated by a black body at the same temperature. Values range between 1, corresponding to the blackbody emitter, to 0, which corresponds to no radiation. For this reason materials with high emissivity are preferred. At the same time radiation is wavelength (λ) and temperature dependent according to Planks law:

$$\mathrm{e}(\lambda) = \frac{2\pi h_p c^2}{\lambda^5 \left[\exp^{\frac{h_p c}{k\lambda T}} - 1\right]}$$

Where e(λ) is the energy, h_p is Planks constant, K is Boltzmann constant and c is the speed of light. As it can be seen graphically plotting energy as a function of wavelength, the peak shifts depending on the temperature of the emitter. Since cells cannot convert the whole spectrum, but only in a certain bandwidth, it is important to have the maximum energy in the correspondent interval. This dependency has brought the adaption of the so called "selective emitters", as shown in Fig. 1.2, taken from Ref.

(5). These particular materials emit not on the whole spectrum but only in a certain range. If this is matched with the cell bandwidth the production of electric power is maximized.

A classification of materials can be made considering four groups:

1. High temperature resistant materials
2. Selective rare earth oxides
3. Photonic crystals
4. Ceramics

This is not intended as an absolute classification, materials could be ordered, for example, concerning emissivity or temperature resistance. The choice of the material depends on the type of cells, the cost and the shape of the emitter. Many works have been done trying to estimate the best configuration emitter - cells and performances have been evaluated in various papers, as in Refs. (6) and (7).

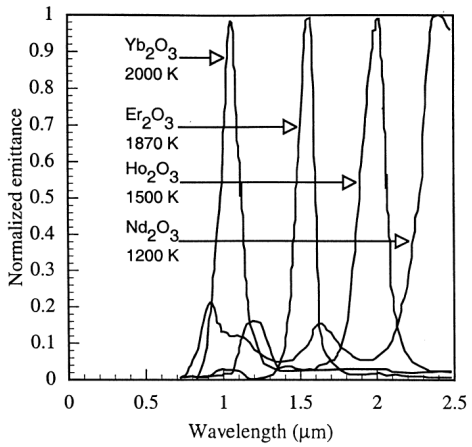

Figure 1.2: selective emitters spectra

Inconel can resist to high temperatures and has values of emissivity ranging from 0.75 to 0.9 depending on the oxidation intensity. Silicon Carbide (SiC) has an emissivity of 0.9 and can resist temperatures up to 1900 K, but energy is distributed through the whole spectrum. Allumina has similar mechanical properties but has lower values of emissivity. Yb_2O_3, on the other hand, is a narrow band, or selective, emitter. It resists to high temperatures and has a peak emission at 1.27 eV, considering a temperature of

1735 K and an emissivity of 0.85, as stated in Refs. (4), (7) and (8). Er_2O_3 has similar performances: emissivity of 0.85 with a peak at 0.8 eV considering a temperature of 1680 K. Other narrow-bandgap materials can be used to match cell response: Holmia (0.6 eV),Neodymia (0.5 eV), for example, as presented in Refs. (5) and (8).

1.3 Cells

Thermophotovoltaic cells are semiconductor devices which absorb radiation and convert it in electricity through the photovoltaic effect. In principle the process is exactly the same as for solar power, but there are two differences regarding the temperature of the emitter and the distance between the source and the cells. The sun, in fact, has a temperature of 4800 K, the emitter, instead does not reach 2000 K. On the other hand the distance drops down to a few centimeters, with a bigger energy density reaching the surface of the cells.

For these reasons solar cells are not suitable for TPV applications and the conversion of radiative energy into electricity becomes a very critical process. Many factors influence power generation, the most important are temperature of the emitter, wavelength, power density and cell operating conditions. It is not simple to define the best configuration in order to obtain the maximum production of electricity because, as said before, it depends on the entire system.

Thermophotovoltaic cells are apparently similar to solar cells, the main difference is that these types of cells are low bandgap cells. In TPV applications emitter temperature is about 1500 K, although some devices reach slightly higher values. With these temperatures the emissive power is low and the most of it is located in the infrared region, at low values of wavelength. So it is important to convert the greatest amount of energy using cells with low bandgap values, in order to match the emissive energy produced by the emitter.

To obtain high efficiency values traditional Silicon and Germanium cells cannot be used because these give an insufficient electrical output. To resolve these problems a wide range of materials and configurations have been tested in the past years. The best performances have been obtained with unconventional materials and multi-layer cells. But still some problems limit the diffusion of these types of cells. The major as cost and toxicity.

GaSb (Gallium antomonide) cells have better characteristics, that can be enhanced combining these with different other materials to form multi-junction cells: GaInSb, GaInAsSb, InGaAs, InAs, InPAs, InAsP,InGaAsSb and InAsSbP. In this particular field research is very active and two configurations are been studied now: InGaAs and InAsP,

epitaxial structures on InP substrates (NREL, NASA-Glenn Research Center) and InGaAsSb epitaxial structures on GaSb substructures (MIT Lincoln Labs, Sarnoff Labs at Princeton University, Sandia National Laboratories), as reported in Ref. (9). InGaAs/InP cell is shown in Fig. 1.3, taken from Ref. (8).

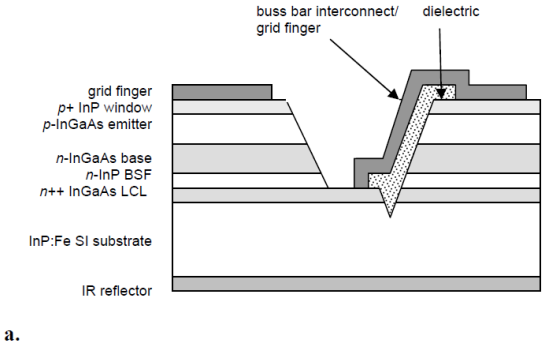

Figure 1.3: InGaAs/InP TPV cells

1.4 Other components

Heat source, emitter and cells are the fundamental parts of the system, but for a correct operation of a TPV device other parts must be included: optical filter, cooling system, heat exchanger and electronic devices. Even though in some cases these are not strictly necessary, performances are by far enhanced, but costs as well.

Filters can be interposed between emitter and cells, introducing two important positive aspects. Basically filters let only a desired portion of the spectrum pass and block the rest. The redirected radiation enhances and stabilizes the emitter temperature,decreases cell temperature, enhancing conversion efficiency. The pass band wavelength must be matched with the bandgap of the cells, thus depends on the configuration adopted. Different types of filters have been studied including plasma filters, dielectric filters and low badgap filters.

As said before, cell efficiency is inversely proportional to the temperature of the back surface of the cells. The proximity of a high temperature heat source and portion of radiation which is not converted leads to the necessity of a cooling system which can be provided by air or in the majority of applications by water.

1.5 Coupling and overall performance

TPV devices have been studied for quite some time now, early developments started in the 90s, since then, different solutions and configurations have been tested. It is difficult to compare all the prototypes since applications regard different destinations, as classified in Ref. (5):

- portable systems
- stand alone devices
- transportation use
- recovery use for industrial waste heat

It is very important to state that every single part has great importance on overall performances. But at the same time coupling between the parts is essential too. This implies finding the best configuration in order to optimize the energy flux in every passage. This can actually be seen as developing the single component having constraints derived from performances of the rest of the system.

Following this approach a series of parameters can be defined to evaluate every passage in the energy flux cascade. It is important to notice that various parameters can be defined and their definition is not unique. Here are reported three different efficiences.

$$\eta_{thermal} = \frac{\int_0^\infty e\left(\lambda\right)}{P_{in}}$$

Regarding the heat source, usually emitter temperature and radiative power are measured. With this value thermal efficiency ($\eta_{thermal}$) can be defined as the ratio between input power and radiated power. This gives an idea on how energy is transformed into heat.

$$\eta_{in-band} = \frac{\int_{\lambda\,\min}^{\lambda\,\max} e\left(\lambda\right)}{\int_0^\infty e\left(\lambda\right)}$$

Another efficiency value can be calculated for the interaction between the emitter and the cells $\eta_{in-band}$, defining it as the ratio between the whole spectrum of radiation and the part of it which can be actually converted by cells, determined by λ_{max} and λ_{min}. This parameter does not take into account the electrical output of the cells. In order to evaluate losses for sub bandgap energy that cannot be absorbed by the cells and the heating of the back surface circuits, other parameters would be needed.

$$\eta_{tpv} = \frac{P_{el}}{P_{in}}$$

If considering the whole system, the ratio between input power and electrical output,η_{tpv}, can be calculated. Since the system has at least five fundamental parts, as Coutts states in Ref. (5), even if having all components at 90 % efficiency singularly, total efficiency would drop to 54 %. This is, although a very optimistic result. In the same article the author states that a 15 % efficiency in short term can be achieved, while a 20 % is a long term objective.

1.6 State of art

Since the early stages TPV systems have remained prototypes developed be laboratories of different countries: JX - Crystals in the U.S. and CANMET in Canada, only to cite two. Nowadays only one commercially available TPV system exists: the Midnight Sun, produced by JX-Crystals. This is a stove for house heating applications, sold between 1998 and 2001 in 20 test units, but then the production had stopped. The Midnight sun used propane as fuel for a nominal input power of 7.5 kW and was able to produce 150 Watts of electric power, out of which 50 W were used to operate blower and fans. The effciency can thus be calculated in 2 %, sa reported in Ref. (10). In the same publication are presented the results of another operating prototype developed in the same labs. This has an emitter temperature of 1275 °C with an area of 469 cm^2. Electrical output has been measured using a single GaSb cell and the performances of the system have been calculated from that value. This would result in a electric power generation of 703 W with an overall efficiency of 16 %, still in Ref. (10).

Figure 1.4: Midnight Sun stove

Qiu and Hayden at CANMET have been very active in TPV research and have published several papers, Refs. (1), (2) and (11]. In their paper several results have

been presented for a radiant burner at several operating conditions using InGaAsSb cells. Tests have been performed with a cell area of 0.004 m^2, this value has then been multiplied considering an active area of 0.00297 m^2. Results are reported for two different cases with the same energy input 6900 W. Case 1 with no air preheating, has a radiator temperature of 1323 K, a power density of 3900 W, leading to a production of 115.8 W of electrical power.Case 2 with a relative preheating of 0.31 %, corresponding to an air temperature of 745 K has enhanced performances. Radiator temperature is increaased to 1463 K, energy density to 5400 W, for an output power of 160.4 W.

Reference (12) presents the results of a miniature thermophotovoltaic device consisting of a burner and GaSb cells. The best results were achieved with a reverse tube for hot combustion products, reaching surface temperatures of about 900 °C with an electrical output of 6 W considering an active cell area of 72 cm^2.

1.7 Costs

The limiting value of efficiency is one of the reasons why TPV systems are still not commercialized, but the most important is by far cost. Emitters, filters and cells all need the use of rare materials, difficult manufacturing processes and delicate assembling. It is difficult to make a correct estimate of the cost of a TPV device since prices are determined by quantity orders and exact geometrical configuration. But an idea can be made considering prices of materials found on some websites:

- Emitter: 150 millimeters Silicon carbide tube costs about 300 euros (www.goodfellow.com)
- Filter: a quartz tube with a diameter of 40 millimeters and a length of 500 has a cost of about 300 euros (www.goodfellow.com).
- Cells: GaSb cells produced by JX-Crystals, having anactive area of 1.48 cm2 cost 40 dollars

1.8 Bibliography

(1) K. Qiu, A.C.S. Hayden, Thermophotovoltaic generation of electricity in a gas fired heater: influence of radiant burner configurations and combustion processes, *Energy conversion and management*, Vol. 44 (2003), pp. 2779-2789

(2) K. Qiu, A.C.S. Hayden, M.G. Mauk, O.V. Sulima, Generation of electricity using InGaAsSb and GaSb TPV cells in combustion driven radiant sources, *Solar Energy Materials and Solar Cells*, Vol. 90 (2006), pp. 68-81

(3) G. Colangelo, A. de Risi, D. Laforgia, Experimental study of a burner with high temperature heat recovery system for TPV applications, *Energy Conversion and Management*, Vol. 47 (2006), pp. 1192-1206

(4) Wilhelm Durisch, Bernd Bitnar, Novel thin film thermophotovoltaic system, *Solar Energy materials and solar cells*

(5) Timothy J. Coutts, An overview of thermophotovoltaic generation of electricity, *Solar Energy Materials and Solar Cells*, Vol. 66 (2001), pp. 443 - 452

(6) Narihito Nakagawa, Hideki Ohtsubo , Yoshiharu Waku, Hiroo Yugami, Thermal emission properties of Al2O3/Er3Al5O12 eutetic ceramics, *Journal of the European Ceramic Society*, Vol. 25 (2005), pp. 1285-1291

(7) K. Qiu, A.C.S. Hayden, Thermphotovoltaic power generation systems using natural gas-fired radiant burners, *Solar Energy Materials and Solar Cells*, Vol. 91, Issue 7 (2007), pp. 588 - 596

(8) B. Bitnar, W. Durisch, J.-C. Mayor, H. Sigg, H.R. Tschudi, Characterisation of rare earth selective emitters for thermophotovoltaic applications, *Solar Energy Materials Solar Cells*, Vol. 73 (2002), pp. 221-234

(9) G. Mauk, Survey on thermophotovoltaic (TPV) devices, School of Engineering and Applied Science, University of Pennsylvania, Philadelphia, Pennsylvania, USA.

(10) www.jxcrystals.com

(11) K. Qiu, A. C. S. Hayden, Performance of low bandgap thermophotovoltaic cells in a small cogeneration system, *Solar Energy*, Vol. 74 (2033), pp. 489-495

(12) Yuenh-Heng Li, Hong-Yuan Li, Derek Dunn-Rankin and Yei-Chin Chao, Enhancing thermal, electrical efficiences of a miniature combustion-driven thermophotovoltaic system, *Progress in Photovoltaics: Research and Applications*, Vol. 17 (2009), pp. 502 - 512

2

BURNER

As explained in the previous chapter, even though the production of electric power is not the main issue, it is important to obtain the highest amount of electricity. Reaching this goal is not a simple task because of the complexity of the system and the phenomena which are involved. Every single component of the system must be matched to the other and all processes must be tuned to work at the best performance. The different ways of coupling emitter, cells and filters will not be treated in this work. In this project only the burner has been developed, so no considerations on the efficiency and performance of the whole system will be considered.

In this chapter the first steps of the design of the burner will be presented. Since it has been decided to develop a completely new configuration, no existing systems have been taken into account. This choice, though, leads to a long and complex development of the burner. Initial targets and objectives have to be defined and, within, several different possible options have to be evaluated. Selected solutions must be tested and optimized to reach the desired performances. In this chapter this initial development is presented, leading to the first prototype of the burner.

2.1 Home application

The first step is the decision of the application or the destination of the TPV system. As said, the device is thought for domestic house heating. In the aim of the project, this kind of device should replace old and less efficient boiler systems. Heating systems must produce:

- hot water at low temperature (< 60 °C) for bathroom and kitchen
- hot water at high temperature (60 °C $< t < 100$ °C) for the heating of the environment

- hot air at low temperature (30 °C < t < 40 °C) for room heating

This is actually the starting point of the development. In fact, a medium European apartment needs about 12 kW of power to guarantee these two needs, considering a maximum demand. In reality this value does not help in dimensioning the burner, since many options are available to reach this value: a single device of 12 kW, two devices in parallel 6 kW each or other possibilities. This is a peak value considered for winter time, in other seasons power request is lower, thus the possibility to have optimal performance at partial loads can be better achieved with a multiple system. Another direct consequence of being a house heating application is the choice of the fuel: methane. This is fed directly by piping to apartments and houses. Other similar fuels could be used for other applications such as portable systems, transportation or stand alone appliances: propane or natural gas, for example.

The geometrical part of the design has been started with the idea of using a pointwise light source. This assumption is based on the necessity of maximizing emissive power density. This is a necessity on one hand and an advantage on the other. Having a low temperature emitter, in fact, requires more concentrated radiation to produce electrical output, which is directly proportional to the energy density reaching the cells. At the same time, considering the same amount of electricity, it is possible to reduce the active area of the cells, thus decreasing the cost of the entire system.

Considering different shapes, the best idea seems to be using a tube. The ideal case would be to have an infinitely small diameter, but obviously this is not possible. With small values, maintaining combustion could be a real issue because of various phenomena. But the increase in surface could bring temperatures to lower values and decrease radiation. As initial guess the diameter has been chosen to be 20 millimeters, although this value can be changed during the development if desired performances are not sufficient. As for the length it has been decided to try with 200 millimeters, giving a total emitting surface of 0.0126 m^2.

2.2 Design

Regarding the combustor, it has to be designed in order to maximize the conversion of thermal power, incoming through the reactants, to thermal radiation leaving the emitter. This depends not only on the geometrical characteristics but also on the materials used and the flow conditions. Despite the aim of the design some important characteristics have to be fulfilled regarding combustion:

1. complete and stable reactions

2. avoid flashback

3. avoid autoignition

When these constraints are observed, then research can be focused on the reaching the maximum electric output. Strictly regarding the burner, four conditions have to be satisfied:

1. high emitter temperature

2. temperature uniformity on the emitter surface

3. large emitter surface

4. within law emissions

To reach the first objective it has been decided to use the combustion chamber outer surface as emitter. This leads to a reduction of the energy conversion steps, which are source of power losses. To have a high surface temperature, convective and conductive heat transfer between the flame and the emitter must be maximized. To achieve this target it is desirable to have the flame near the walls of the combustion chamber, attached if possible. Regarding the flow characteristics it is important to have higher velocity values near the boundaries and lower corresponding to the centerline. This is the opposite situation respect almost all other burners, where the walls are kept at low temperatures, with the flame positioned in the center of the combustion chamber.

Temperature uniformity is difficult to define since it can have different values and importance, depending on dimensions, cells connectivity and temperature values. In fact, there are many conflicting aspects to be considered, and a compromise has to be found between them. Enhancing the emitter area will decrease temperature uniformity, which will decrease maximum values of emissive power. This is only one example from which a decision has to be made, considering the final electrical output.

The main issue is exactly defining the characteristics of the cell circuit. In fact, the type of the cells and their connectivity is not known. The cells are connected in series and parallel in order to have power output at desired levels of current and voltage. These values for cells are defined by the elementary cell which sees the minimum temperature, thus conditioning the rest. For this reason uniformity is very important.

In order to have a uniform temperature over the whole radiator the flame front has to be stretched and corrugated. In this way the contact surface between the emitter and the flame is greatly enhanced. To do so it is impossible to use a laminar flow field, but turbulence has to be imparted to the flow before entering in combustion chamber. The

enhanced motion of the fluid flow is a positive aspect not only for the stabilization of the combustion reaction but even for the mixing process of air and gas.

All these considerations led to the choice of using a swirling flow. This particular type of motion is characterized by rotation and strong values of axial and tangential velocities in the outer part of the tube. Depending on the swirl intensity, in correspondence of the centerline of the tube a inner core vortex with negative axial velocity values can form. These characteristics perfectly fit this application. In several applications regarding combustion and heat transfer swirl has been used for different pourposes. Descriptions can be found in Refs. (1) - (7).

Regarding combustion, and in particular the feeding of reactants two choices are availible: premixed and non-premixed combustion. In the first case air and fuel are fed and mixed before the entrance of the combustion chamber. While in the second, the diffusion takes place directly near the zone of the ignition of the flame. It has been preferred a premixed reaction in order to better control the process when partial loads are involved. Furthermore, in this way it is possible to limit pollutant formation in some cases.

2.3 Geometry

The burner has been designed in order to have appropriate geometrical characteristics in order to develop a stable combustion in a swirling flow field. All dimensions are thought to be consistent with the combustion chamber diameter. Moreover it has been tried to limit the overall dimensions of the burner, especially axial length could have created some problems. To overcome this issue, it has been decided to force the flow to accomplish two reversals. In fact, the whole burner is 300 millimeters long and has a maximum width of 80 millimeters. The entire TPV system, than, considering the heat exchanger, cells and the auxiliary systems should have limited dimensions, which is definitly a good characteristic. In this chapter the first prototype is fully described, in the next chapters results regarding experimental tests and numerical simulations will be presented.

The burner can be divided into 5 zones, as shown in Fig. 2.1:

(1) air inlet

(2) gas inlet

(3) swirler

(4) mixing zone

(5) combustion chamber

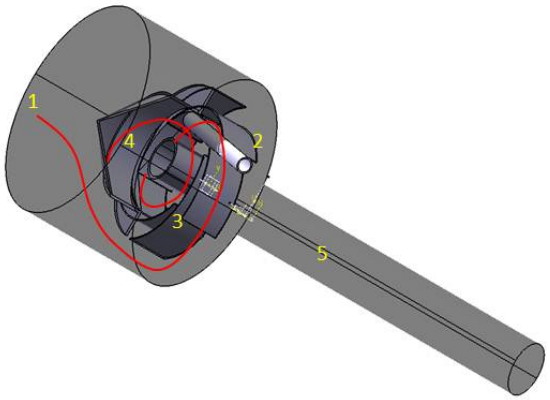

Figure 2.1: 3D image of the burner

The inlet consists of a 80 millimeter diameter tube, which also has the function of containing the flow. At the end of the tube the flow gets reversed for the first time and is forced to go through radial vanes. These have a circular shape and create a anti-clockwise spin, if looking at the flow from the inlet. A three dimensional representation can be seen in Fig. 2.2. There are different ways of imparting swirl to a flow, among which tangential inlets, rotating parts or vanes are only some. For this application radial vanes seemed the best choice since a strong swirl intensity can be imparted and at the same time no moving parts are involved. This leads to lower costs and especially less maintainance problems. To generate sufficient swirl 6 vanes have been used. In a previous work a configuration with only 4 vanes had been tested but the flow field had worst characteristics and so was rejected.

Figure 2.2: Drawings of the tangential palette

The rotating stream is forced then to pass in the annular region delimited by the hood and the inner tube. In this area gas is injected inside the rotating flow through

a 5 millimeter tube, placed radially inside the burner. Propane is dragged by the fluid stream inside the burner and the reactants start to mix. The diffusion process takes place inside what can be defined as the mixing zone, labeled with number 3 in Fig 2.1. This step is very important, since the ignition and the stability of the combustion reactions depend on the diffusion of the molecules of gas in the air stream. Both dimensions and velocity values influence the mixing process. The ratio between these two characterstics can be analyzed through the residence time. In fact, if the space is not adequate or the flow is fast the reactants will not have enough time to diffuse, but on the other hand, if the space is large or velocity small the flow will lose the swirling motion.

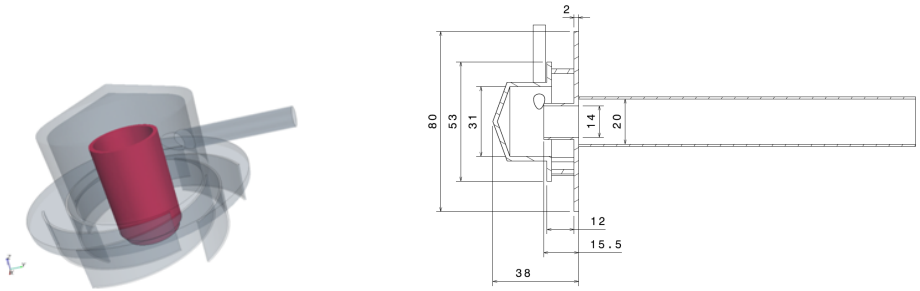

Figure 2.3: Inner tube and section plane of the burner

In the mixing zone the flow is reversed a second time, hitting the cone shape of the hood. Then air and gas are forced to enter inside the 14 millimeter diameter inner tube, shown in Fig. 2.3, left. This part is essential to create a discontinuity in flow area and create an abrupt expansion at the entrance of the combustion chamber, as can be seen from the section of the burner in the right hand side of Fig. 2.3. This choice has the aim of deflecting the streamlines towards the walls of the combustion chamber enhancing heat transfer from the flame to the surface. Moreover at the outer zone of the abrupt expansion an area of low velocity is created, which should act as ignition and anchoring zone for the flame.

2.4 Bibliography

(1) P. Palies, D. Durox, T. Schuller, P. Morenton, S. Candel, Dynamics of premixed confined swirling flames, *C. R. Mecanique*, Vol. 337 (2009), pp. 395-405

(2) D.G. Sloan, P.J. Smith and L.D. Smoot, Modeling of swirl in turbulent flow systems, *Prog. Energy Combustion Science*, Vol. 12 (1986) , pp. 163 - 250

(3) O. V. Mitrofanova, Hydrodynamics and Heat Transfer in Swirling Flows in Channels with Swirlers (Analytical Review), *High Temperature*, Vol. 41, No. 4, (2003), pp. 518-559

(4) P. Weigand, W. Meier, X.R. Duan, W. Stricker, M. Aigner, Investigations of swirl flames in a gas turbine model combustor I. Flow field, structures, temperature, and species distributions, *Combustion and Flame*, Vol. 144 (2006), pp. 205-224

(5) Yehia A. Eldrainy, Khalid M. Saqr, Hossam S. Aly, Mohammad Nazri Mohd Jaafar, CFD insight of the flow dynamics in a novel swirler for gas turbine combustors, *International Communications in Heat and Mass Transfer*, Vol. 36 (2009), pp. 936-941

(6) E. C. Fernandes, M. V. Heitor and S. I. Shtork, An analysis of unsteady highly turbulent swirling flow in a model vortex combustor, *Experiments in Fluids*, Vol. 40 (2006): 177-187 DOI 10.1007/s00348-005-0034-4

(7) Yuenh-Heng Li, Hong-Yuan Li, Derek Dunn-Rankin and Yei-Chin Chao, Enhancing thermal, electrical efficiencies of a miniature combustion-driven thermophotovoltaic system, *Progress in Photovoltaics: Research and Applications*, Vol. 17 (2009), pp. 502 - 512

3

LASER DOPPLER VELOCIMETRY

Experimental testing is a fundamental part of every design and optimization process. In fact, it is essential to have reliable data to validate numerical simulations and understand whether the system effectively works. For both reasons it is important to collect as much information as possible.

In the design of this TPV system CFD simulations have a relevant part, since it is possible to obtain important information. As it will be seen in the next chapters, this kind of numerical analysis is affected by various errors. If the flow is turbulent, a consistent part is due to the turbulent model used. In fact, implemented models are not case specific and use a series of constants tuned to predict correctly a wide range of velocity fields. But these can fail in case of complex flows, for example affected by strong rotation, as in this burner.

In this chapter experimental tests on the burner with non reacting flow will be presented. In order to determine the characteristics of the flow field many techniques are available. All can be divided in two classes: intrusive and non intrusive. Hot wire anemometry, Pitot tube measurements, for example, belong to the first since instruments modify the velocity and pressure values in the nearby space. Particle Image Velocimetry (PIV), Laser Doppler Velocimetry (LDV or LDA), instead, belong to the second class because with these techniques it is possible measure the flow field from outside the region of interest.

Different measure techniques can be used in this case. Thermal anemometry would be very difficult to use in this case for several reasons. First of all the instrument has to be calibrated, operation which has to be repeated after several measures. And although it has a very fast response, this technique is directionally ambiguous, which for recirculating flows could be a problem.

Using Pitot tubes could be a problem too, for the limited dimensions of the combustion chamber. Introducing a probe inside the tube would certainly modify the values of axial and tangential velocity. In this particular case, where recirculation is likely to occur, flow field after the probe influences what happens in front of it, leading to incorrect measurements.

LDV on the other hand is a non intrusive technique, since measures are done using laser beams. It is directionally sensitive and no calibration is needed, since it is an absolute measurement technique. Other aspects have to be checked in order to have precise results, but these will be analyzed in the next sections.

3.1 Theory

In this section some theoretical aspects of the Laser Doppler Velocimetry will be presented. For a full description of principles and details many articles and presentations can be found, as Refs. (1) and (2). This technique is based upon light scattering from tracer particles. A LDA system is made up of a laser, transmitting optics, receiving optics and signal processor. Laser light is used because it is coherent, monochromatic and has low divergence. In a dual beam configuration the laser light is divided in two beams of thickness D_L, which pass through a transmitting lens and intersect at a certain distance, F, from the source, as can be seen in Fig. 3.1, taken from Ref. (2).

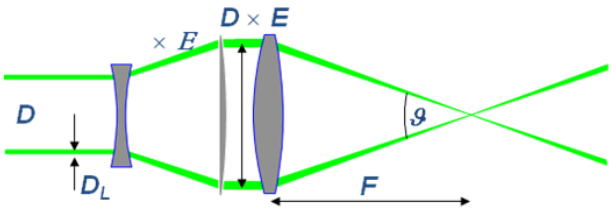

Figure 3.1: Beam configuration

The two coherent beams intersecting create the ellipsoidal shape measuring volume, consisting of a fringe pattern of bright and dark lines. Dimensions of the volume are determined by F, wavelength (λ) and the configuration of the system, where E represents the amplification factor and θ is the angle between the two laser beams. Dimensions of the ellipsoid, height (x), width (y) and length (z) are calculated through the following equations:

$$x = \frac{4F\lambda}{\pi E D_L \cos(\theta/2)} \qquad y = \frac{4F\lambda}{\pi E D_L} \qquad z = \frac{4F\lambda}{\pi E D_L \sin(\theta/2)}$$

The frequency of one of the beams is shifted using a Bragg cell, this allows to have a moving fringe. This is done in order to determine the direction of the moving particle. In fact, light, reflected by the seed, has a lower frequency if it moves in the same direction as the flow, while it has a greater frequency if it moves in the opposite direction.

Errors can arise using this technique: the velocity bias error, the gradient bias error and the Doppler ambiguity error. When particles have different velocity values, the faster ones will travel through the measurement volume in shorter time. So a greater number of fast particles will be detected and the velocity value will be upward biased. The gradient biased error has the same theoretical basis as the velocity error. The only difference is that it affects measures near the walls where the shear layer is present. The Doppler ambiguity is an error caused by having a limited number of particles measured during the time interval and is a statistical type of error.

The Mechanical Department laboratory is supplied with an argon laser generator produced by Coherent, shown in Fig. 3.2. The model is a Innova 90 Plus with a maximum power of 5 Watts. The rest, consisting of a transmitter, manipulators and probe, are products of Dantec Dynamics. The laser has been operated with powers ranging from 1 to 1.8 Watts. The two light components are green at 512.5 nm and blue at 488 nm. These characteristics bring to a focal distance of 310 mm for an angle of 7.35 degrees. There is no separate receiving photodetector since the laser operates in the backscatter mode. Seeding was provided by liquid glicerine particles nebulized by a homemade device.

Figure 3.2: Innova 90 Plus laser

3.2 Results

At first, measures have been tried with the first prototype of the burner equipped with a PVC transparent tube for optical access of the combustion chamber. But some problems made it impossible to perform measures in that case. In fact, the walls of the

combustion chamber would get very soon dirty in correspondence to the expansion in the combustion chamber, where tangential and centrifugal forces are very strong. Bigger particles collide with the inner surface of the tube and slide on it, leaving a layer of dust. This would interfere with the laser beams, reflecting part of the light and leading to a very low signal. The limited dimensions of the combustion chamber gave furthermore problems in measures in the near wall region, where it is difficult to measure points close the surface of the wall.

For these reasons it has been decided to build a bigger model using Reynolds similarity. The new diameter of the tube has been brought to 50 millimeters, thus enlarging the system by a factor of 2.5. The length of the combustion chamber is now 750 mm. The new value of air flow rate is 450 l/min.

In the measuring line air is fed by a centrifugal 1.5 kW fan. The flow is then forced to pass through a honeycomb which straightens the flow inside a 3 meter long tube. At the beginning of the PVC tube glycerine particles are injected in the fluid stream. These particles are nebulized inside a seeder, where the fluid stream is accelerated inside a nozzle. The difference in velocity creates a low pressure zone which sucks the particles from the lower part of the seeder into the high speed flow. Then the flow passes through a cyclone separator where the bigger particles are eliminated.

To have a complete velocity profile inside the combustion chamber a total number of 84 points in the radial direction have been measured, at every axial location. Since points very close to the wall are very difficult to obtain, it has been preferred not to take them into account. Traverses are taken at 5 different axial locations: 1D, 2D, 5D, 10D and in correspondence of the sudden expansion, at the entrance of the combustion chamber. Due to the very turbulent nature of the flow, measuring time has been increased to 20 - 30 seconds depending on the location of the point, with a maximum number of bursts of 10000 particles. This leads to a total time of 45 minutes for every single traverse.

The location of points has been corrected to take into account the deviation of the trajectory of the beams due to the curvature of the tube. Both the horizontal and the vertical direction in each axial location have been measured, to check simmetry and precision of the acquisition.

Measures gave some problems due to the turbulent and rotating nature of the flow. The Burstware software which supports the acquisition of data has several functions and parameters which can be used to analyze the quality of each measure. Among these, the most important are: the histogram chart, mean value, the root mean square (rsm) value, the skewness, the flatness factor and the turbulent intensity as defined in Ref. (3). To judge the quality of the traverse measure it has been decided to compare the calculated value of the mass flow rate, found integrating the profile through the whole section and

the value measured by the flow meter. If the error exceeded 5%, the measure had to be repeated. Considering then every single acquisition point, the minimum number of particles passing through the measuring volume has been checked. In order to consider the result valid, at least 5000 particles have to cross the ellipsoid . The histogram gives an immediate image on the distribution of the value of velocity, from this mean and statistic quantities can be extracted. Mean value is simply sum of the velocity values divided by the number of particles. Increasing the sampling time allows more particles to pass through the measuring volume, but on the other hand this enhances the probability to have droplets at different velocities. For this reason it has been decided to limit to root mean square value to 5 in order to consider valid the measure. In this way it is not necessary to apply any correction for the velocity bias error.

Since this is a symmetrical flow considering the centerline of the combustion chamber tube two aspects can help to judge results: similarity between the velocity profile obtained through the measure of a horizontal and vertical traverse and the symmetry between points at the same distance from the origin. Qualitatively the first aspect can be seen in Fig. 3.3.

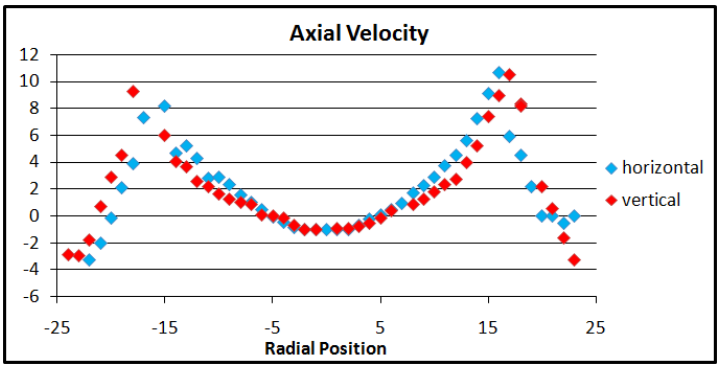

Figure 3.3: Axial velocity profile

The velocity profile is very similar, even though some differences can be seen between 8 mm and 15 mm in radial location, while in correspondence of the ceterline, results are almost identical. The difference can be due to a physical aspect regarding the instability of the inner core vortex which has a slight oscillation frequency, thus results are time dependent. The other is a geometrical difference due to the diffraction of the beams caused by the curved surface of the tube. So both the horizontal and the vertical traverse are not centered at the centerline of the combustion chamber.

Comparing the velocity distribution it can be seen good agreement betweeen the left and the right hand side, as shown in Fig. 3.4. Considerations proposed for the previous

case can be extended to this case with similar conclusions.

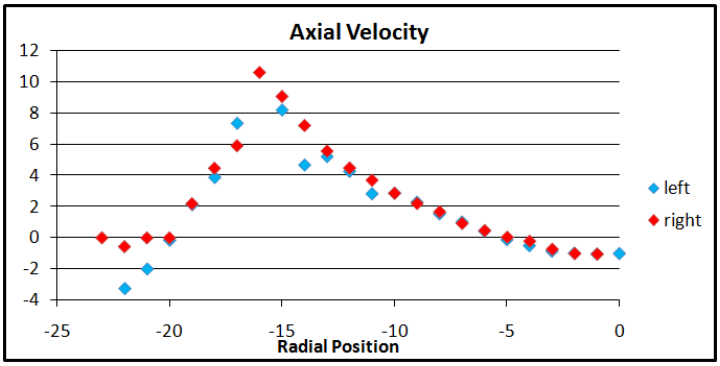

Figure 3.4: Specular axial velocity profile

Tangential velocity acquisition on the other hand was very complex. In fact, reliable data was obtained only considering the horizontal traverse, as shown in Fig. 3.5. Results from the vertical one were unrealistic, both regarding values and shape of the flow. In this case, simmetry in values is not always respected.

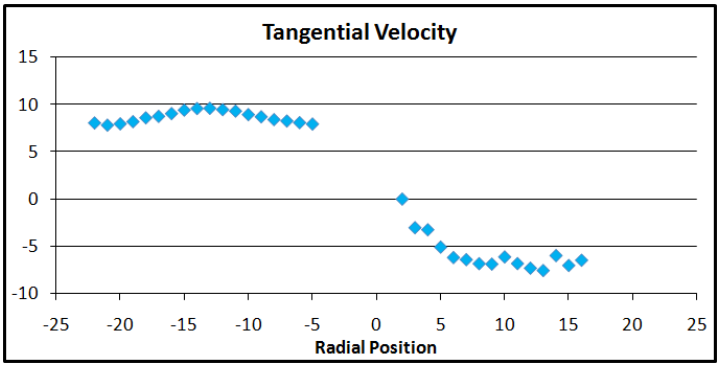

Figure 3.5: Tangential velocity profile

Figure 3.6 shows the axial velocity profile of the 0 D measure, in correspondence to the expansion at the entrance of the combustion chamber. As it can be seen velocity has a peak value corresponding to the radial location of 16 mm, which corresponds to the radius of the inner tube. On the external region a stagnation zone is present, where velocity drops down to negative values. This underlined the existence of a small vortex. In correspondence of the centerline of the tube an inner core vortex 10 mm wide in the radial direction can be observed. It has to be said that measures in this location

have been very trivial, in fact, some points did not fulfill the imposed requirements for root mean square or turbulence values. Regarding the tangential component of velocity, measured have failed in all points except for few. Several adjustments have been tried to obtain correct results. Time of analysis was increased in order to have more particles, frequency has been enhanced, but still problems have been not overcome.

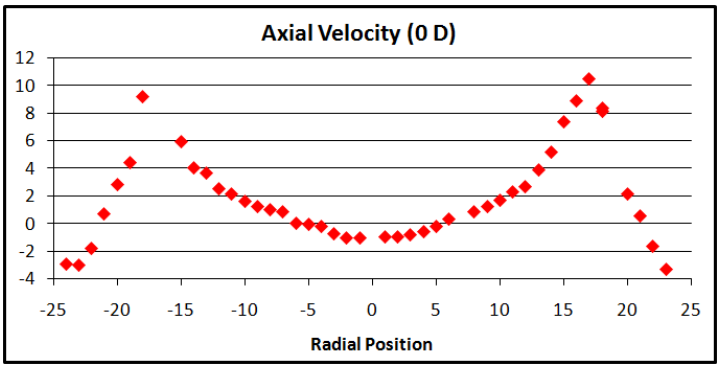

Figure 3.6: Axial velocity profile at the entrance of the combustion chamber

Measures in axial direction corresponding at 100 millimeters (2 D), 250 millimeters (5 D) and 500 millimeters (10 D) all show similar trends. In Figs. 3.7 and 3.8 are shown respectively the profile of axial velocity at 100 millimeters and 500 millimeters from the entrance of the combustion chamber. Comparing measured values at the entrance, three differences can be seen. The positive peak value has now decresed from 12 m/s to 6 m/s, the location in the near wall region, where the stagnation zone is no more existing. As a consequence the inner core vortex has more strenght and the negative velocity has a value of -4 m/s. It is interesting to note that the recirculation zone keeps a constant strength through out the entire length of the combustion chamber, this means the swirl intensity is mantained.

Concluding it can be said that this experimental test has been done with success. The Laser Doppler Velocimetry has been used to determine characteristics of the fluid flow. Axial and tangential profiles have been detected and can be used to tune the CFD turbulence model. Important information has been gained on this type of swirling flow. Further tests will have to be performed with reacting flow, in order to gain some knowledge on the combustion reactions and determine how these influence the flow field characteristics.

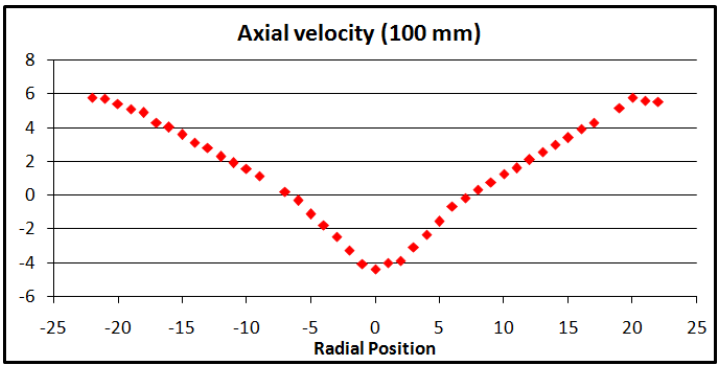

Figure 3.7: Axial velocity at 100 mm from the entrance of the combustion chamber

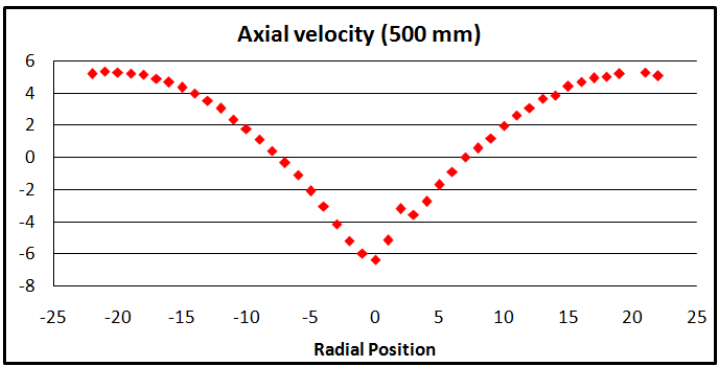

Figure 3.8: Axial velocity at 500 mm from the entrance of the combustion chamber

3.3 Bibliography

(1) Gerta Rocklage-Marliani, Maren Scmidts, Venkatesa I. Vasanta Ram, Three dimensional laser Doppler velocimeter measurments in swirling turbulent pipe flow *Flow, Turbulence and Combustion*, Vol. 70 (2003), pp. 43-67

(2) www.dantecdynamics.com

(3) Burstware Operating manual, *Dantec Dynamics*

4

CFD NON REACTING FLOW

As said in the previous chapters, turbulence and swirl are very important features in this application, in order to optimize and stabilize the combustion process. This necessitates a correct prediction of the principal characteristics of the fluid flow. Immediately performing simulations of the reactive case could lead to a difficult analysis of errors and incorrect results. Having at the same time combustion, turbulence, radiation and heat transfer, discerning the various contributions to the total error would have been a real issue. In order to isolate errors due to the turbulence model, CFD simulations of the non-reacting flow have been performed. In this chapter this work and relative results are presented.

In order to test various turbulence models validation has been done comparing results with data obtained in the experimental tests. As explained in the previous chapter, the burner dimensions have been changed, because precise measures on the real burner had not given satisfactory results. Experimental data have been used to judge the numerical results and a comparison will be here presented.

In the first section of the chapter a review of the basic principles undergoing computational fluid dynamics will be presented considering only some general aspects. For more explanations several books, as in Ref. (1), (2) and (3), websites, Ref. (4) and articles, Ref. (5), can be read. This swirling turbulent flow is particular and complex due to its rotational nature. For this reason various models have been tested in order to understand which performs best in this particular case. First classical models were tested, moving then to more complex simulations. For each simulation the grid independence study, the comparison with experimental data and the analysis of the results are fully presented in the second section. Finally in the last section the flow field considering the real dimensions of the burner is analyzed.

4.1 Computational fluid dynamics

Computational fluid dynamics is the study of fluid flows using numerical codes.In principle the domain of interest is divided into elementary volumes, called control volumes. Computationally the fundamental equations are solved for every control volume in an iterative way. This means the solution is updated at every step and is said to be converged when the error between two consecutive steps, called residual, is below a user defined value.

In CFD the prediction of turbulence is still a challenge due to the chaotic and stochastic nature both in space and time. In order to analyze the evolution of a fluid flow, the characteristics can be divided in a mean and a turbulent component. Using this decomposition in the equations of flow, as said before, some terms arise: these terms are called Reynolds stresses. In order to solve the dynamics of the flow, three approaches exist:

- Reynolds Averaged Navier-Stokes Equations (RANS)
- Large Eddy Simulation (LES) and Detached Eddy Simulation (DES)
- Direct Numerical Simulation (DNS)

Only the DNS technique resolves directly the equations, but it can only be applied to simple cases with very low Reynolds numbers. The LES and DES both have to same principles and solve the flow in a detailed way through filtering procedures. RANS techniques use the Navier Stokes equations and are used very often because respect to the others have a lower computational cost.

These three techniques have advantages and disadvantages. Many discussions on which is the best approach have been made and many different opinions on the matter exist. Summarizing it is possible to say that Large Eddy Simulation is more precise, gets more details and is able to predict quantities RANS does not. On the other hand it is extremely costly in terms of computational time and resources and is not so straightforward for very complex systems. For this reasons RANS equations are still very popular in industrial environment, where time is the primary issue and, often, mean quantities are sufficient. LES has been developed in academic institutes in order to have a better insight in fluid and combustion dynamics, as has been presented in Ref. (6) . But now, with the increasing power of super computers it has been applied for particular industrial pourposes.

Direct numerical simulation (DNS) is more costly then LES. In this case mesh size and time step must be very small in order to include all structures and fluctuations, for this reason DNS is limited to a very broad number of cases, considering small Reynolds

numbers and simple geometries. Just to have an idea, it is known that both quantities depend on the Reynolds number with a power law:

$$N_{grid} \propto \mathrm{Re}^{9/4} \qquad N_{timestep} \propto \mathrm{Re}^{3/4}$$

Focusing on RANS, there are two possibilities to solve the Reynold stress terms or the "closure problem"′ as it is usualy defined: model the Reynolds stresses considering another variable or model them directly and separately. The first method consists in modeling the unknown stresses through other terms. In the second case all the terms of the fundamental equations are modeled. A total of seven equations have to be solved, thus greatly increasing complexity and time of the problem. The principal models are listed below:

- one equation: Spalart - Allmaras
- two equation: k - epsilon and k - omega
- seven equation: Reynolds stress model

For one and two equations models in order to solve the Reynolds stresses, these quantities are linked to the turbulent kinetic energy k with the so called Boussinesq approximation:

$$\rho \langle u_i u_j \rangle = 2\mu_t S_{ij} - \frac{1}{3}\rho k S_{ij} \qquad k = \frac{1}{2}\left(u_1 u_1 + u_2 u_2 + u_3 u_3\right)$$

Reference (1) states that this is a simplicistic formulation and is expected to fail with complex flows involving rotation and anisotropy.

4.2 CFD code

The numerical simulation was performed using the software STAR CCM+, developed by CD-ADAPCO, and explained in Ref. (7). The software allows to perform all the operations needed for the study: creating the geometry, generating the mesh, putting up the physical problem, solving the differential equations and postprocessing the results. In this particular case the geometry has been done with CATIA VR5 and then imported inside the code in iges format.

Simulations have been run on a workstation at the Department of Mechanical Engineering of the University of Trieste. It is a Dell T7500 model with two Intel(R) Xeon(R) quad core processors E5620 and 32 gB of RAM memory. This allows to run the simulation with up to 8 parallel processors, decreasing sensibly the computational time. Despite this, to complete a simulation takes from about 20 hours using the k-epsilon model to about 40 performing the simulation with a Reynolds stress model.

4.3 Models

Different Reynolds Averaged Navier Stokes(RANS) models have been tested. K-epsilon in its standard formulation was the first to be investigated because it is the most used of the two equation models. Then the k-omega model was used to see if it was able to predict in a better way streamline curvature. Then the Spalart-Allmaras one equation model was used to see if computational time saving would lead to a worsening of the results. At the end the more complex and computationally intensive 7 equation Reynolds Stress model has been tested. This test has been done for swirling flows and results have been published in several papers, for example in Refs. (8), (9), (10) and (11).

All simulations have many common characteristics: three dimensional, stationary and steady. Especially this last hypothesis is not completely correct if considering the time dependent properties of swirling flows. But in order to achieve good results with the simplest model possible, flow is considered to stabilize at regime, this means that the flow is studied in fully developed conditions. This approximation seems to be confirmed by experimental tests, in which temperature changes on the emitter oscillate for only 5 $°C$ - 6 $°C$. Air was used as working fluid, considered as ideal gas, mixture of 21 % of oxygen and 79 % of Nitrogen . In the case of non reacting flow, with low velocities, density remains constant. But testing turbulence models for combustion simulation, the option of compressible flow seemed more correct.

Another important issue is whether using a coupled or segregated method to resolve velocity-pressure dependence. In literature it is possible to find many accurate explanations on the argument, so here no theory will be presented. In a coupled flow model the mass and momentum equations are solved concurrently, while in the segregated model these are solved independently, as explained in Ref. (7). The first approach has a higher computational cost, needing much more physical memory. For low Mach number incompressible flows a segregated approach is usually preferred, although not in all cases. For example in Ref. (12) the SIMPLEC method has been used. In the non reacting case a segregated approach has been preferred, while the combustion reactions will be maybe modeled using a coupled approach.

In order to compare, in a more objective way results, fundamental criteria, suggested by Pope in Ref. (13), will be used:

- level of description
- completeness
- cost and ease of use

- range of applicability
- accuracy

In this particular case the last criterion is the most important since several methods of the same family have been compared. The others would be considered only in the choice between the methods with comparable accuracy.

4.4 K-epsilon model

K-epsilon is a two equation model which solves the turbulent length scales with the dissipation approximation. It is very widely used model due to its simplicity and applicability. As stated by Versteeg et al. in Ref. (1), this model does not have to capability to predict correctly swirling and rotating flows driven by anisotropy and extra strains.

As usual, the first step in a CFD analysis is a grid independence study. Several meshes have been tested in order to have a full independence of the solution from the spatial discretization. The fluid domain is discretized with polyhedral and prism layer boundary cells. The unstructured mesh has been generated with the automatic mesher available in STAR CCM+. Due to geometrical complexity, it would have been very difficult to create a structured mesh, especially in the passage between the curved blades. Moreover using RANS models a structured mesh was strictly not needed, as it is known that the solution is not very influenced by mesh type but rather by its size.

The first generated mesh is a combination of a unstructured and a extruded grid. As first step a unstructed polyhedrical mesh was generated in the swirler zone. In order to try to minimize the number of cells, but at the same time optimize the cell distribution, different cell size in different zones was used. In the entrance zone, where only laminar flow is present, a base size of 4 mm was chosen. Subsequently a local refinement has been performed in the mixing zone, where the flow is complex and velocity gradients are intense. Base size is reduced to 2 mm. For the entrance of the combustion chamber an extruded mesh was built. In the validation procedure, in fact, it was seen that this type performs better results especially when the Reynolds stress model was applied. The length of the extrusion was set to 745 millimeters, 372 layers were built with the same dimensions. Prism layer mesh have been used on boundaries with customized values depending on flow characteristics and importance in computing precise results.

Fundamental characteristics of the coarse mesh are:

- number of cells: 767580
- number of faces: 3331229

- number of vertices: 2081343

Analyzing results it can be seen that residuals are low. All have values of the order of 10^{-4} except for the turbulent dissipation rate which is $7.39 * 10^{-4}$. Presumably running the simulation for more iterations, this value would have been further reduced, but the solution was already stabilized.

A second mesh was generated, resulting as a refinement of the first one. The only parameter which has been modified, in the swirler zone, is the base size, the new value has passed from 4 millimeters to 3 millimeters. At the same time the extruded mesh parameters have been changed in the number of layers, passing from 372 to 497. All the other parameters do not change as they are related in percentage to the fixed base size.

Fundamental characteristics of the medium mesh are:

- number of cells: 1684299
- number of faces: 7465161
- number of vertices: 4700795

The third generated mesh is a new refinement of the second mesh, but only in the combustion chamber and the swirler zone. The number of layers are now 745, having thus a length of 1 millimeter each. The cell size in the swirler zone is now of 1 millimeter leading to a fine mesh of:

- number of cells: 3955574
- number of faces: 18298369
- number of vertices: 9458220

To see the effect of mesh type a fourth grid was generated. This time it is a fully unstructured grid, which means no extruded mesh, has been generated this time. This could be seen as an unnecessary step, since the k-epsilon is not so sensitive to grid type. But in order to compare these results with other types of models, it was important to be sure solution was not linked to the extrusion type mesh. The last mesh has these characteristics:

- number of cells: 1851489
- number of faces: 11173953
- number of vertices: 8900031

Results of the three space discretizations have been analyzed and compared in order to decide which mesh is the best compromise between a correct solution and computational time. The table below contains values used to analyze the independency of the solution from the spatial discretization. Results for the fully unstructured mesh have not been presented since these do not differ respect the second mesh, which has a similar number of control volumes.

data	zone	mesh 1	mesh 2	mesh 3
area shear stress	CC wall	0.9356863	0.8903486	0.8634229
volume averaged velocity	combustion chamber	5.476622	5.574580	5.619518
volume averaged velocity	swirler zone	1.690920	1.718362	1.722209
maximum axial velocity	swirler zone	11.46191	11.57075	11.33964
maximun axial velocity	combustion chamber	8.007352	8.431321	8.652018

Table 4.1: grid independence study

Values of velocity, shear stress and pressure, which are not reported here, change very little from one mesh to the other. Velocity profiles are the same, just very little differences due to mesh size are visible. Velocity and pressure fields have been qualitatively analyzed and the same conclusions can be done. No macroscopic differences can be seen plotting the results on a section plane through the whole combustor. This means that solutions for the medium and fine grid are in the asymptotic range.

The y+ value was investigated in the whole domain. In the swirler values are very large for the coarse mesh, but are acceptable because a two-layer k-epsilon model was used, as described in Ref. (7). In order to try other types of models, prism layer thickness and number of layers has to be incremented in order to have maximum values of about one. Decreasing, in the medium and fine mesh, cell size, values of y+ decrease. In both cases in the combustion chamber values are around 0.8, which can be judged as very good. So an error cannot be due to the modeling of the viscous sub-layer.

The outlet boundary condition is very important in order to get good results and to compare them with experimental data. It influences CFD results depending on the condition which is chosen. For this reason it would be desired to put the outlet boundary as far a possible to the location of points of interest by enlarging computational domain respect physical space. Obviously, this cannot be done, because it would lead to an increase of computational time and resources.

In order to investigate the influence of the outlet boundary condition on the flow inside the combustion chamber, a simulation modeling external environment has been carried out. In fact, truncating the flow space at the end of the combustion chamber, can

produce a numerical error if reversed flow is present and as seen in experimental results the inner recirculating vortex is still present at the end of the tube. Using a pressure outlet boundary condition in presence of inflow is not actually correct as stated in Ref. (7). Comparing the results from this last simulation with the others, some difference arise. Since this is the more correct approach, the results with the external environment will be used to compare experimental data.

Concluding, the second mesh is good compromise between computational time and results. Comparing CFD and experimental results we do not find good agreement, as can be seen in Figs. 4.1 and 4.2. Especially in the center of the tube experimental tests show a strong recirculation vortex. In numerical simulations this cannot be seen. The rotation of the flow is, in fact, understimated, as can be seen in Fig. 4.2 too.

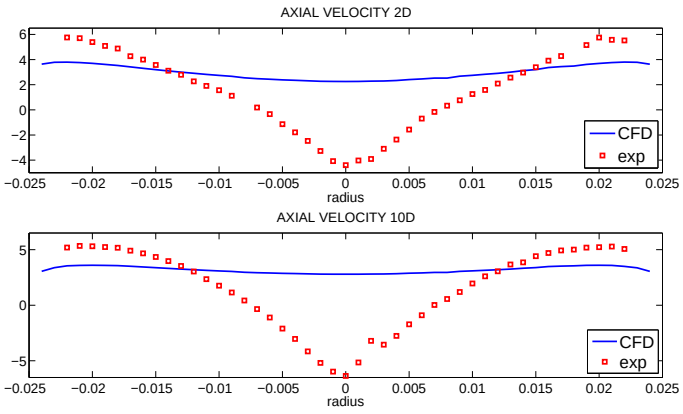

Figure 4.1: Axial velocity profile predicted with the k-epsilon model

In order try and reduce the error, two different variants of the k-epsilon model available in STAR CCM+ have been tested. These two models have a quadratic and cubic relation to describe the Boussinesq approximation. As stated in the user manual, Ref. (7), these two relations should account better for the anisotropy of the flow. Still with these other models the ability to predict rotation of the flow mainly depends on the model constants, which, for better results would have to be tuned for the particular case of analysis. In fact, both the quadratic and the cubic method failed to predict the inner recirculating vortex. Actually worse results were obtained respect the standard k-epsilon model.

Concluding it can be said that, despite changing several parameters, the k-epsilon model fails to simulate correctly the flow inside the mixing zone and the combustion chamber. Comparing CFD and experimental results we do not find good agreement.

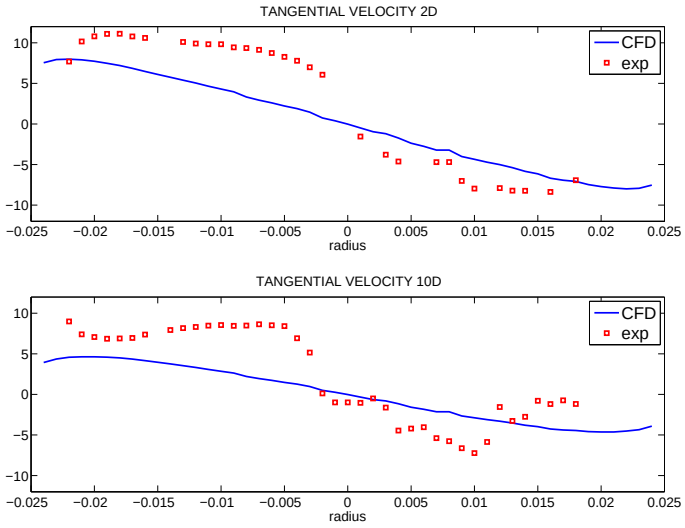

Figure 4.2: Tangential velocity profile predicted with the k-epsilon model

Especially in the center of the tube experimental tests show a strong recirculation vortex, which in numerical simulations cannot be seen. Wall treatment, domain discretization, model variants have all be tested, but no improvement has been achieved. For this reason it can be said that the failure of this type of model is due to the theoretical basis on which it rilies. In order to get good results other turbulence models will be tested.

4.5 K-omega model

This two equation model is based on the computation of the kinetic energy and the specific dissipation, omega. It has been used because it should better predict swirling flows compared to the k-epsilon model. As in the previous case a grid independence study has been performed. The generated mesh is similar to the one used in the k-epsilon case. Refined polyhedrial cells are been generated in the swirler zone, while an extruded type mesh is built in the combustion chamber. Since the procedure has been explained in detail for the previous model, in this and the next cases only results will be presented.

Comparing numerical predictions with experimental measurements it can be seen that this model, as the k-epsilon, fails to predict the inner recirculating zone. No negative axial velocity values are seen in the centerline of the tube, while with LDV tests values up to -4 m/s have been measured. The difference of velocity values is shown in Fig. 4.3,

for the the 2D and 5D horizontal traverse.

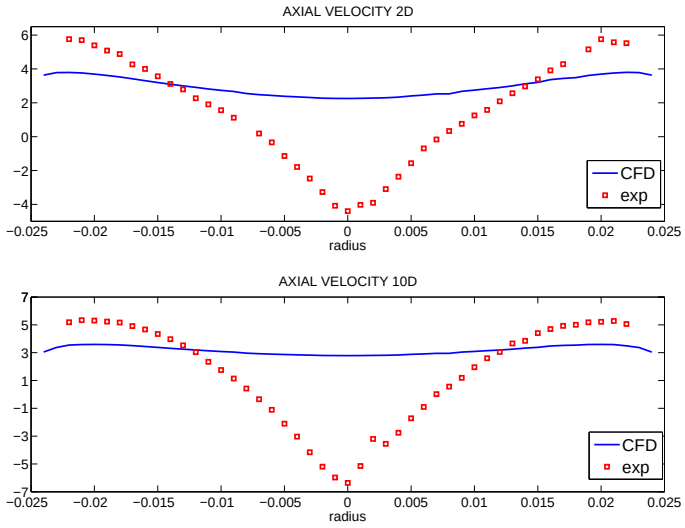

Figure 4.3: Axial velocity profiles predicted with the k-omega model

In the last version of STAR CCM+ 8.02.008, a new variant of the two equation model has been implemented, in order to account for rotation of the domain and curvature of streamlines of the flow. This new approach is based on a correction factor, described in Ref. (7), following the work done by Durbin et al., as explained in Refs. (13) and (14). In the usual k - ω SST Menter model the two scalar equations have the form:

$$\frac{\partial k}{\partial t} + u_j \frac{\partial k}{\partial x_j} = P - \varepsilon + \frac{\partial}{\partial x_j}\left[\left(\nu + \frac{\nu_T}{\sigma_k}\right)\frac{\partial k}{\partial x_j}\right]$$

$$\frac{\partial \omega}{\partial t} + u_j \frac{\partial \omega}{\partial x_j} = \frac{\gamma}{\nu_T} P - D_\omega + \frac{\partial}{\partial x_j}\left[\left(\nu + \frac{\nu_T}{\sigma_\omega}\right)\frac{\partial k}{\partial x_j}\right] + CD_\omega$$

The eddy viscosity is calculated through an expression using the kinetic energy, the kinetic dissipation and a constant C_μ, which has a unity value and does not take into account rotation or streamline curvature. A first modification was introduced in Ref. (13) with a new coefficient C_μ^*, the same concept has been then modified by Arolla and Durbin presented in Ref. (14). In the CFD code the formulation, described in Ref. (7), is implemented as:

$$C_\mu^* = C_\mu f_c = C_\mu \left(\min\left(C_{\max}\frac{1}{C_{r1}\left(|\eta| - \eta\right)} + \sqrt{1 - \min\left(C_{r2}, 0.99\right)}\right)\right)$$

$$\eta = \tau^2 \left(S : S - W : W\right) \qquad C_{\max} = 1.25 \qquad C_{r1} = 0.04645 \qquad C_{r2} = 0.25$$

With the curvature correction results better match the experimental data obtained with the laser measurements. As it can be seen in the velocity profile, the inner core vortex, characterized by negative axial velocity, is now predicted. Figures 4.4 and 4.5 show, respectively, the axial and tangetial velocity profiles at different axial locations inside the combustion chamber. Applying the correction sensibly improves the prediction of the inner recirculating vortex. At 250 mm results match, while at 100 mm the numerical model overstimates the negative values at the centerline of the tube. On the other hand, the opposite occurs at 500 mm, where results are underestimated by the numerical simualtion. As for the first case this could be due to an error in the viscous sub-layer in the wall region. The second incongruity may be caused by the modeling of the external environment and the boundary conditions.

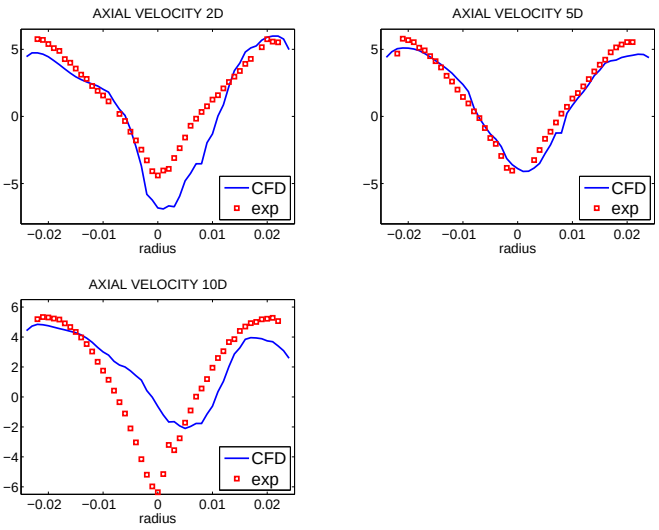

Figure 4.4: Axial velocity profiles predicted with the k-omega SST Menter formulation with curvature correction

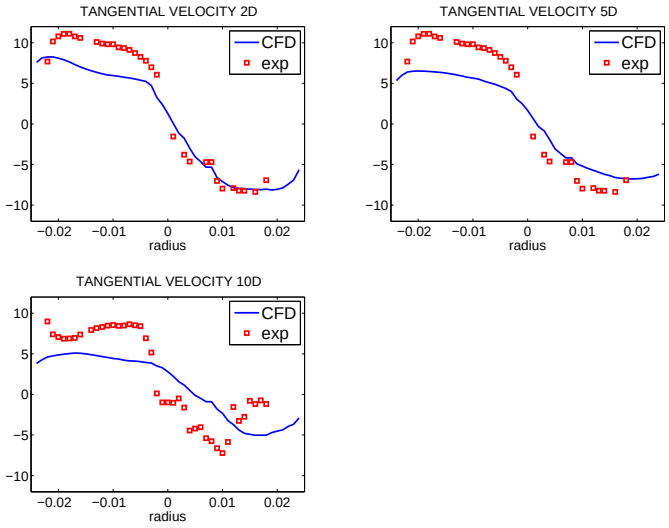

Figure 4.5: Tangential velocity profiles predicted with the k-omega SST Menter formulation with curvature correction

4.6 Spalart-Allmaras model

In this section results are presented for the Spalart-Allmaras turbulence model. This is a one equation model, which solves a transport equation for turbulent viscosity, detailes can be found in Refs. (1) and (2). At first sight, this could be thought as less accurate respect to the two equation models. But that is not completely true, because it does not solve for the turbulent kinetic energy, thus not requiring any specification for the characteristic length scale. This model was developed for aerodynamic calculations, but can be used with success to other types of flow. Comparing it to other models, having only one equation to solve it is less expensive computationally.

A fully unstructured mesh of polyhedrial volumes has been used, as previously. Flow and boundary conditions are the same as in the other simulations. In STAR CCM+ three variations of the model are implemented. In this case a standard formulation of the Spalart-Allmaras model has been used, coupled with an all y+ wall treatment. To get good convergence first an upwind advective scheme was used untill residuals would drop down to the order of 10^{-3}. Then, using the obtained solution as starting point, a second order scheme has been used until the solution would be converged.

A grid independence study was performed, in order to check the independency of the

solution to the space discretization. The coarse grid has 1227016 cells, corresponding to a base size of 2.3 millimeters. For the medium grid base size was decreased to 1.8 millimeters, leading to 2143011 cells. Finally in the fine mesh the number of cells was increased to 3086359, with a base size of 1.5 millimeters. To check grid independence various quantities have been analyzed. Upon these, shear stress at the combustion chamber wall and mean velocity in the whole fluid domain are listed in the table 4.2. Mean extracted values show little difference, analyzing specific results show that the asymptotic range for solution variation is obtained for the medium mesh.

mesh	shear stress	velocity	total CPU time (s)
coarse	0.304276	1.659602	72150
medium	0.3354095	1.742116	85614
fine	0.341158	1.761546	158109

Table 4.2: grid independence results

Even though using a blending function to treat the viscous sub-layer, wall y+ has been checked for the three meshes. In all of them at the combustion chamber walls values did not exceed unity. For all the other boundaries maximum values never exceeded 6 in the worst quality mesh. Since a reversed flow at the exit, which actually is an interface of the external environment, was present, mass flow rate was checked in all three cases. Values were very close to the nominal rate, thus numerical errors can be considered negligible. Residuals are very low in the whole domain. The maximum values for x, y and z momentum residuals in the fluid domain are respectively $3.876 * 10^{-5}$, $4.775 * 10^{-5}$ and $4.776 * 10^{-5}$. Velocity and pressure values have been checked during the calculation in order to verify that the solution had reached the steady state, so that the flow field was completely developed.

Comparing experimental data with values from the CFD simulation, shown in Fig. 4.6, it is possible to see a good correspondence. Axial velocity values at 2 D from the inlet of the combustion chamber are overlapping. Moving towards the exit, velocity profiles differences start to arise, and the underestimation of the numerical simulation increases. As for the previous models, the CFD simulation predict a decying swirling flow, while the experimental tests suggest a constant rate of rotation throught the whole combustion chamber. Considering the flow field at 5 D, differences are localized in two areas. In the near wall region numerical results predict a value of 4.2 m/s against the 5.8 m/s of the experimental tests. At the centerline of the tube the negative value of 4.7 m/s is not acheived by CFD, which predicts - 2.3 m/s. Instead from a radial location of 15 millimeters to 5 millimeters, results match perfectly.

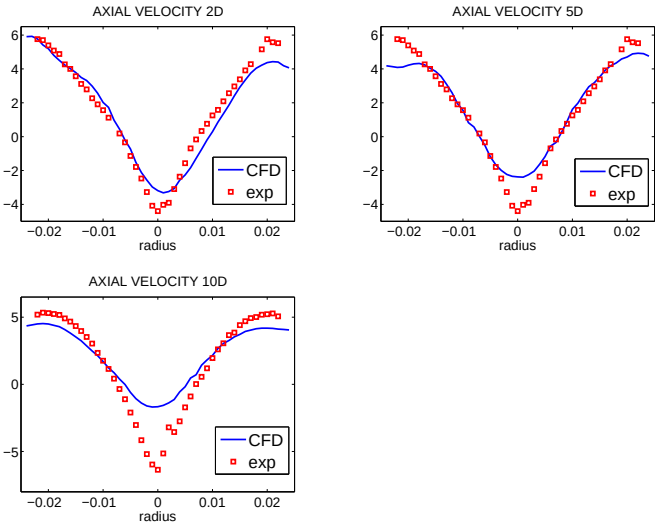

Figure 4.6: Axial velocity profiles predicted with the Spalart - Allmaras model

Tangential velocity profiles have to be compared too. As seen from Fig. 4.7, experimental data e CFD results do not quite overlap. This is not really to attribute to the simulation models, but to the uncertainty regarding the experimental tests, as desribed in chapter 3. Measuring this velocity component in the radial direction was quite trivial. In fact, in many points the measure resulted really impossible for lack of enough particles, too high route mean square values, both probably caused by the deflection of the beams due to the changing and increasing curvature of the wall when reaching the upper and lower points of the combustion chamber.

Results using the Spalart-Allmaras model gave unexpected results. Even though it is based on the solution of a single equation, the prediction of the swirling motion of the flow is predicted. The comparison with experimental data shows a better accurancy respect the k - epsilon and the k - omega with no correction for curvature. Computational time is lower in order to achieve a converged solution. Unfortunatly this model is not supported in the combustion simulation, so it cannot be used for the reacting flow case. For this reason, this model could be used only to run a geometrical optimization regarding the mixing of reactants, within a week time on more powerful machine, if the flow field considering the combustion reactions would be modified in a limited way.

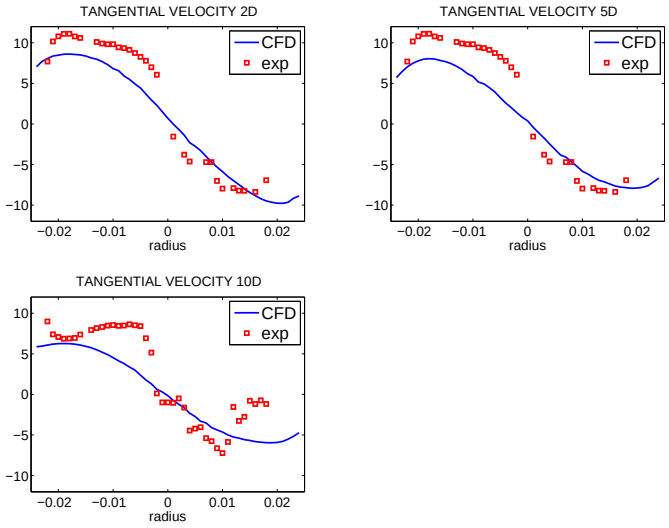

Figure 4.7: Tangential velocity profiles predicted with the Spalart - Allmaras model

4.7 Reynolds stress model

The Reynolds stress model is the most complete model in the RANS methods family. It accounts for all the stresses individually and thus solves one equation for each individual stress. Due to this complexity, computational time largely increases using this kind of method. But for research purposes results contain a large variety of information, which can help to better understand fluid flow characteristics.

One the major problems using the RSM model is the convergence of the solution. For this reason some values were kept under control during simulation and then all were analyzed. Maximum value of the x - momentum, y - momentum and z - momentum residuals in the domain are respectively $1.544 * 10^{-5}$, $2.202 * 10^{-5}$ and $5.221 * 10^{-5}$. All the values of the maximum Reynolds stresses residuals in the fluid domain are listed below:

- uu $= 6.8397 * 10^{-5}$ vv $= 5.3911 * 10^{-5}$ ww $= 7.0079 * 10^{-5}$
- uv $= 1.3359 * 10^{-5}$ uw $= 2.5228 * 10^{-5}$ vw $= 2.7885 * 10^{-5}$

As done previously three meshes have been tested to ensure grid independence of the solution. The fine mesh has an extruded grid in the combustion chamber leading to a total number of 3955574 cells for the fine mesh.

Axial velocity profiles are in good agreement with experimental data, as shown in Fig. 4.8. Analyzing the first traverse it can be seen that the negative peak value is not in correspondence to the centerline of the combustion chamber. Due to this asymmetry results from the right part of the velocity profile fit better experimental results respect to the ones of the left side. This result can be accepted since in other numerical and experimental works this phenomenon has occured or been numerically simulated. Looking at the 5D profile results quite overlap and only slight differences in values can be seen in the processing core vortex zone. Moving towards the exit, at 500 millimeters from the entrance of the combustion chamber, the Reynolds stress model undersetimates the negative velocities in the inner core vortex. Since even the Spalart - Allmaras model and the k - omega SST Menter with the curvature correction both underestimated in the way as the Reynolds stress model the velocity profile towards the exit, it is likely that this error is due to some other kind of approximation.

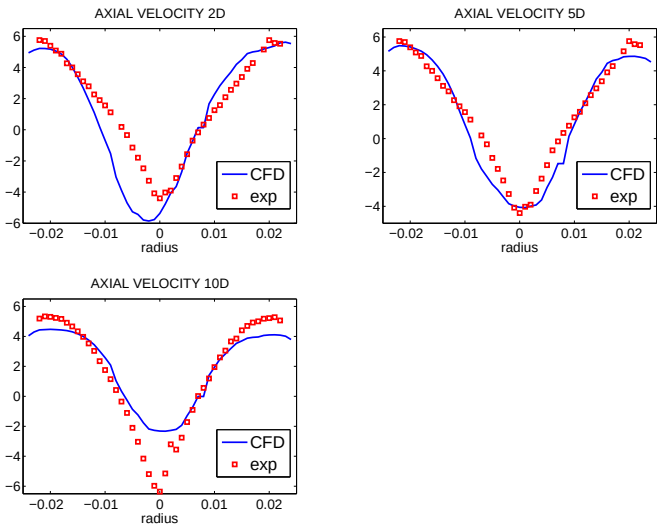

Figure 4.8: Axial velocity profiles predicted with the Reynolds stress model

The tangential velocity profiles are shown in Fig. 4.9 for the axial locations at 100, 250 and 500 millimeters from the sudden expansion. Of all the tested methods the Reynolds stress model has to best results compared to data achieved with the LDV technique. The 2 D traverse, in particular, has overlapping values. In both the other profiles, the left hand side values are underestimated by the numerical model.

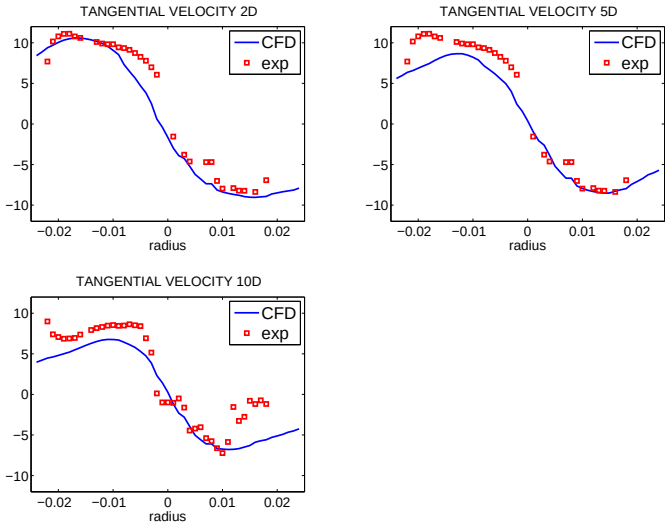

Figure 4.9: Tangential velocity profiles predicted with the Reynolds stress model

4.8 Conclusions

Several numerical models for the prediction of the turbulent flow have been tested. Among the ones implemented in STAR CCM+ three have been able to correctly predict the swirling motion inside the burner. These are the Spalart - Allmaras, the k - omega SST Menter with curvature correction and the Reynolds stress models. For the analysis of the burner in operating conditions the one equation model cannot be used, since it is not supported by the combustion option. The choice will be between the remaining two other models.

After having tested the turbulence models on the bigger prototype, a numerical simulation regarding the burner with the correct measures has been run, using the Reynolds stress model. Plotting the axial and tangential velocity on a section plane through the whole combustor, important characteristics about the flow can be seen in Figs. 4.10 and 4.11. As expected flow characteristics are similar, since the experimental prototype had been designed using the flow similarity.

There is a reverse flow zone, with negative values of axial velocity, located at the centerline of the combustion chamber tube, called processing core vortex. These characteristics are found till the end of the combustion chamber, indicating that the swirl is maintained through the whole length. At the inlet of the tube, the sudden expan-

sion generates the stagnation zone characterized by a low intensity vortex. This is the region where the flame should ignite. The core vortex enters inside the swirler till the mixing chamber. This can be seen as a positive aspect. In fact, hot products will tend to recirculate in the zone heating up fresh gases and enhancing flame stability.

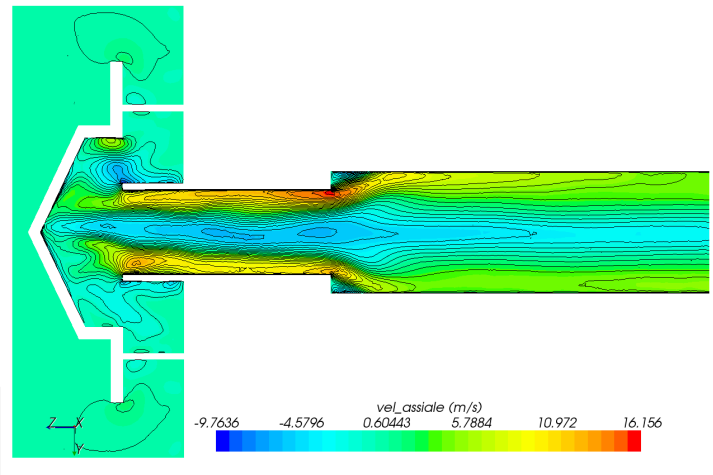

Figure 4.10: Axial velocity values on a section plane

From both axial and tangential velocity plot it can be seen that there is not a perfect symmetry in the section plane considering the centerline of the tube. The reason is probably to be attributed to some grade of unsteadiness of the flow.

In order to have a good insight of the flow the Q-criterion values have been analyzed. The Q-criterion is very useful in order to see where the flow is rotating and where it is not, identifying in this way coherent structures. Mathematically the Q-criterion is a scalar, as described in Ref. (7). If the Q parameter is positive the rotation rate, vorticity, dominates over strain rate. As expected, the Q-criterion is positive in almost the whole combustor. Negative values are present only the boundary regions, close to the walls.

Helicity is another important parameter in order to understand fluid motion. In a swirling flow if streamlines evolve in a left handed skrew, the value of helicity is positive. On the other hand if it is right handed it is negative. Due to the geometrical characteristics of the swirl generator, it can be easily said that a left handed skrew is expected and thus a positive value of helicity in the outer part of the combustion chamber.

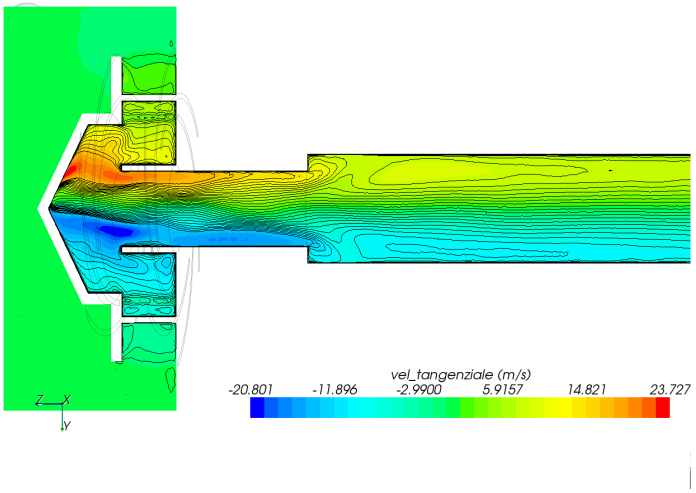

Figure 4.11: Tangential velocity values o a section plane

4.9 Bibliography

(1) H. K. Versteeg and W. Malalasekera, An introduction to computational fluid dynamics: The finite volume method, *Pearson*, second edition (2007), ISBN-10: 0131274988

(2) Joel H. Ferziger and Milovan Peric, Computational Methods for fluid dynamics, Springer, third edition (2002), ISBN: 3540420746

(3) David C. Wilcox, Turbulence modeling for CFD, *La Canada*, third edition (2006), ISBN: 9781928729082

(4) www.cfd-online.com

(5) Y. Wu, D.C. Haworth, M.F. Modest, B. Cuenot, Direct numerical simulation of turbulence/radiation interaction in premixed combustion systems, *Proceedings of the Combustion Institute*, Vol. 30 (2005), pp. 639 - 646

(6) Lecture Series on Turbulent Combustion, *Von Karman Institute for Fliud Dynamics*, 21 - 25 March 2011

(7) STAR CCM+ user manual, www.cd-adapco.com

(8) Andrew Escue, Jie Cui, Comparison of turbulence models in simulating swirling pipe flows, *Applied Mathematical Modeling* (2010)

(9) Amit Gupta, Ranganathan Kumar, Three-dimensional turbulent swirling flow in a cylinder: experiments and computations, *International Journal of Heat and Fluid Flow* Vol. 28 (2007) pp. 249 - 261

(10) David G. Sloan, Philip J. Smith, L. Douglas Smoot, Modeling of swirl in turbulent flow systems, *Progress in Energy Combustion Science*, Vol. 12 (1986), pp. 163 - 250

(11) S. Murphy, R. Delfos, M. J. M. Pourquie, Z. Olujic, P.J. Jansens, F.T.M. Nieuwstadt, Prediction of strongly swirling flow within an axial hydrocycole using two commercial CFD codes, *Chemical Engineering Science* Vol. 62 (2007), pp. 1619 - 1635

(12) S. B. Pope, Turbulent Flows, *Cambridge University Press*, 2000

(13) B. A. Petterson-Reif, P. A. Durbin, A. Ooi, Modeling rotational effects in rotation in eddy viscosity closures, *International Journal of Heat and Fluid Flow*, Vol. 20, pp. 563 - 573

(14) Sunil K. Arolla and Paul A. Durbin, Modeling rotation and curvature effects within scalar eddy viscosity model framework, *International Journal of Heat and Fluid Flow*, Vol. 39 (2013), pp. 78 - 89

5

EXPERIMENTAL TESTS

Experimental work is fundamental in every engineering process in order to validate, verify numerical simulation results and study aspects of the physical process. This study has been performed at the laboratory of the Department of Engineering and Architecture of the University of Trieste. A prototype has been built and successfully tested in different operating conditions. Data regarding temperature profiles on the combustion chamber has been collected and post processed to obtain some information on combustion dynamics inside the burner. Three different operating conditions have been considered:

(1) No combustion chamber: unconfined combustion in ambient air

(2) Inconel combustion chamber: effective operating conditions

(3) Quartz combustion chamber: visualization of the flame

5.1 Instrumentation

Referring to the burner geometry, already described in chapter 2, two separate inlets are present for gas and air. Air is fed in the axial direction through an 80 millimeter opening. In order to have a uniform flow at the inlet of the burner a 1.2 meter PVC tube has been used. The length considered, being 15 times the diameter, should be enough to get rid of most of the turbulence inside the flow. No straightener or honeycomb has been constructed because the flow characteristics mostly depend on the burner geometry when entering the combustion chamber. Air flow, supplied by a compressor, is regulated by a digital flow controller, commercialized by Bronkhorst High Tech. It belongs to the EL-FLOW series (F-203AV) of high precision and accuracy instruments designed for laboratory testing. These instruments have a bypass, where flow is heated and temperature is measured by a sensor. From the temperature difference and the physical and chemical

characteristics of the fluid, mass flow rate is obtained. Power is supplied through an RJ45 cable in continuos electricity at 24 volts, while regulation is provided through the related software on a desktop computer, linked with the flow controllers with an RS 232 cable.

Gas, instead, is tangentially injected in the burner after air has passed through the swirler. As for air, propane is metered by the same type of controller, only with different flow ranges (F-201AV). Calibration is provided by Bronkhorst for both propane and methane, so no corrective factors have to applied during measurements. Propane is fed from a commercially available gas bottle, unfortunately, the exact lower calorific values is not known or could be obtained from the producer. A guessed value has been calculated from the presumed composition and data obtained in literature.

In both lines pressure reducers have been used in order to feed the flow meters at their nominal pressure, 2/3 and 4/5 bar, for gas and air respectively. Filters guarantee a protection against dust particles and condensation, for a dry and clean flow. A no return valve has been used only in the gas line to prevent flashback for safety reasons. Plastic PVC Rilsen tubes and gas proof junctions have been installed in order to prevent leakages.

In these first tests only temperature measurements have been performed. In fact, temperature distribution on the emitter surface is one of the key issues in the design of a burner for thermophotovoltaic application, as it directly determines the final electric output produced by the cells. As said before, not only temperature maximization is an issue, but uniformity as well. This leads to the necessity of measuring at the same time many points on the combustion chamber outer surface. To achieve this result different instruments can be used:

- Thermocouple
- Temperature sensitive paint
- Optical pirometer
- Infrared thermal camera

Each technique has advantages and disadvantages, without getting into details it can be said that the infrared thermography seems to be the more sutable in this case. In fact, it is a non intrusive measure, at the same time single spots, lines and different areas can be monitored. Images afterward can be easily post processed to get the information needed without repeating the measures. For these reasons this last technique has been used to measure temperature profiles on the combustion chamber outer surface.

All bodies emit radiation at different wavelengths (λ), according to Wiens law depending on temperature:

$$e(\lambda) = \frac{2\pi h_p c^2 \varepsilon}{\lambda^5 \left[\exp\left(\frac{h_p c}{k_B \lambda T}\right) - 1\right]}$$

Where $e(\lambda)$ is the wavelegth dependent energy, h_p is Wiens constant, c is the speed of light, ε is the emissivity and K_B is Boltzmanns constant. Integrating this quantity over the whole spectrum it is possible to obtain the total energy radiated by the emitter. The IR sensors array, measures the incoming radiation over a limited portion of the spectrum, including wavelengths from 3.5 microns to 5 microns or from 8 microns to 12 microns, depending on the type of sensor. The software uses Wiens or Plancks law to find the temperature of the emitting surface.

Measures have been taken with an Agema 470, which has a dedicated software for acquisition, visualization and post processing of the images (Thermocam Researcher). Temperatures can be measured up to 2000 °C with a resolution of 320 x 240 pixels, characteristics are presented in Ref (1). A K-type thermocouple has still been used to measure exhaust gas temperature regarding some configurations. To have a qualitative image of the combustion chamber, pictures have been taken with a digital photocamera.

Figure 5.1: Agema 470 IR thermocamera

5.2 Error estimation

Experimental data acquisition is always affected by errors due to precision of the instruments and to the uncertainty in properties and values of variables. The accuracy of measurements is very important in order to estimate the precision of the collected data, this is of fundamental importance in order to compare results with theoretical analysis or other experimental work. In this section uncertainties affecting input variables and measured data will be analyzed.

Considering flow parameters, errors can be neglected. In fact, mass flow measurements have an accuracy of 1 % and a repeatability of 0.2 %. The only other unknown parameter regarding the flow properties is the lower calorific value, but this affects only efficiency and not the temperature measurement.

Temperature measurements on the other hand are effected by errors: both systematic and random. The Agema 470 has an accuracy of 2 % or 2 degrees, this could lead to errors of about +/- 20 °C for highest measured temperatures of the order of 1000 °C. But this is not the only source of error, uncertainty is affected by the absorbance along the optical path between the object and the thermal camera and from surface parameters. The software inside the Agema 470 has a correction function for the first aspect concerning ambient temperature, humidity, and object distance. These three parameters can be easily determined and affect temperature reading in a not determining way.

The most important cause in uncertainty is material emissivity. In fact, this value depends on the surface material composition, roughness, and oxidation in case of metals. Steel, for example has an emissivity of 0.08 when it is polished, 0.69 when red or rusty, 0.8 oxidized, 0.88 strongly oxidized up to 0.96 for rough surface, as listed in Ref. (2). In order to have more insight on the sensitivity of the temperature values measured considering the input parameters some studies have been made. Each of the four parameters have been chamged singularly to see the influence. Reference values have been taken as:

- emissivity = 0.8
- distance = 1.0 m
- air temperature = 25 ° C
- relative humidity = 40 %

First the emissivity was changed between 0.7 and 0.95. Results are shown in table 5.1. Errors affecting temperature measures are very sensitive to the value of emissivity, relative errors have been calculated dividing the difference with temperature regarding an input value of 0.8.

emissivity	max temp	rel error	mean temp	rel error
0.70	1013	11.2	980.2	19.7
0.73	993.1	8.9	887.8	8.4
0.75	961.2	5.4	861.5	5.2
0.78	934.9	2.5	841.3	2.7
0.80	912.2	0	819.0	0
0.82	900.1	1.3	809.4	1.2
0.85	877.8	3.8	794.1	3
0.87	858.7	5.9	775.8	5.3
0.90	841.2	7.8	754.7	7.9
0.95	810.4	11.2	728.7	11

Table 5.1: Temperature and measure errors for different emissivity

For the other parameters it is different, in fact all can be measured with precision and easily, even though the aim of this test was to see how the temperature was influenced by these. As it can be seen, values change of less then 10 °C, error which depends on the instability of the swirling combustion inside the burner. In fact, the change of mean temperature determined by distance is only 1.2 °C considering 0.8 meters and 1.2 meters. Enhancing ambient temperature by 10 °C leads to an increase of 5.4 °C and varying humidity from 40% to 60% a 6.3 °C difference in mean temperature can be measured.

To determine to correct emissivity of the combustion chamber first all the tubes have been oxidized running the burner, then, while measuring the outer surface temperature with a thermocouple, the emissivity has been changed in order to match the value measured with the IR thermal camera. This procedure has been repeated several times in order to get a real value. Emissivity was determined to be 0.8. This value has been checked during the measures and it has been seen to be constant. This value might change slightly, due to non uniform oxidation, for this reason it is expected a 15 / 20 °C confidence interval, which has to be summed with the thermo-camera error. This leads to a total estimated error of about +/- 35 °C.

There is another unexpected source of uncertainty, which actually was noticed after some measures. Looking at temperature profiles measured by the IR thermal camera, a irregular oxidation of the combustion chamber outer surface was seen. Small spots and bigger zones at different colours could be easily seen in the IR images and in the temperature profile. This problem could not be solved even trying different solutions, a uniform oxidation on two of the three tubes was not acieved, although the used com-

bustion chambers have been obtained cutting pieces of a single tube. Probably there are slight changes in chemical and physical properties of the inconel. Dealing with high temperatures and a constant emissivity value leads to large errors in the estimation of the temperature profile. Attempting a local correction for these spots has been discarded because there is not a unique way of doing it. Temperatures could be corrected considering a higher emissivity than the reference one, leading to lower temperatures, or a lower emissivity, leading to the opposite case. Averaging could be done, but not knowing once again the local value of emissivity, it could bring to even larger errors.

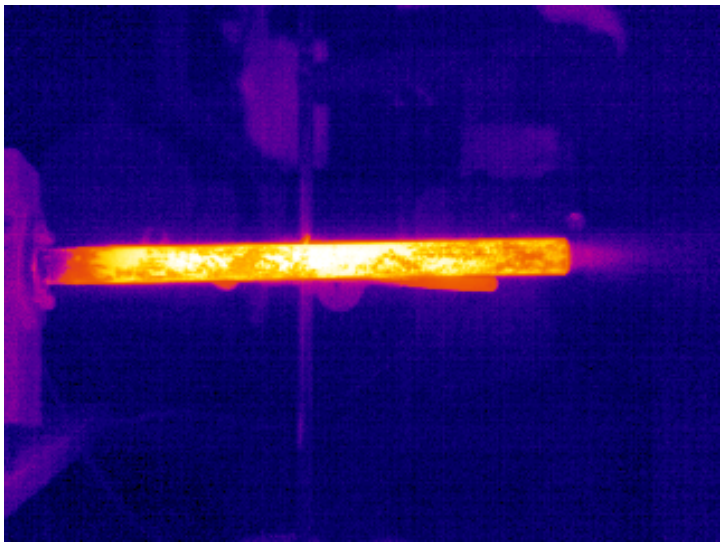

Figure 5.2: IR thermo-camera picture of the tube characterized by spots with different oxidation

5.3 Free flame

The first test has been done without the combustion chamber. The flame was free to burn in ambient air without any constriction. Although this case has no practical interest for the TPV system, it can give some important information on the combustion dynamics.

Rotation and the swirling motion of the flux can be seen from the starting point of the flame till the end of it. It was interesting to notice that the flame ignition point was not located in correspondence of the inner tube exit, but inside. In the original design, the sudden expansion was used to create a recirculation zone with low values of velocity,

where the flame could attach to the wall surface. The ignition of the flame inside the burner is due to the presence of a limited region where fuel and air are already mixed with the low velocity. Unfortunately it is not possible to see the flame front inside the combustor, thus no information about this can be obtained.

5.4 Inconel combustion chamber

This test corresponds to the actual operating conditions of the burner when part of the TPV system. Probably this material will not be used for the combustion chamber, preferring others as Silicon Carbide (SiC) or Allumina, which have higher emissivity and more suitable chemical and mechanical properties, as explained in Ref. (3). In order to collect information on flame stability, ignition, quenching and emitter temperature values, different geometric characteristics and operating conditions have been tested. Referring to the burner geometry, as introduced previously, three parameters have been changed:

1. inner tube length: 16 and 18 millimeters
2. support tube length: 16,12,8,0 millimeters
3. combustion chamber length: 100, 200,300, 300 with holes millimiters

The inner tube length effects the volume of the mixing chamber, keeping the other geometrical values constant. Referring to the geometry of burner presented in chapter 3, increasing the length of this part, the mixing region will decrease. If this area is too small, reactants will not have sufficient time to diffuse in a uniform mixture. On the other hand, if the zone is too big, it will act as an expansion chamber and the flow will lose its swirling characteristics and the rotational component.

The support tube and the inner tube length both determine the total length of the 14 millimeter diameter tube. This variable determines the flow characteristics when entering the combustion chamber. It is not simple to guess the influence of this parameter on the flow characteristics. An increase in length can lead the velocity to get a jet shaped profile at the expense of the tangential component. This influences the flame shape, stretching, impact point on the combustion chamber walls and the strength of the inner core vortex as well.

The combustion chamber length influences strongly the dynamics of the combustion reactions inside the chamber. This is a very important parameter since area and temperature of the outer surface both influence electric power output. Both quenching and heat transfer phenomena influence the dynamics of the flame and the propagation of the

reactions. During the first tests it has been seen that the 300 mm configuration was not performing well. So during the measures it has been decided to try some modifications on the tube in order to enhance combustion stability. Two different type of flame holders have been tried, but none worked. Then, 4, 1 millimeter diameter, holes have been drilled at 25 millimeters from the entrance of the combustion chamber. This modification enhances the stability of the burner, results for this particula configuration will be analyzed in detail in the next sections.

The first two variable values were combined obtaining a matrix of 8 design points, each of which, have been measured changing the length of the combustion chamber. This leads to a total number of 32 different tested configurations. In order to investigate ignition and stability characteristics, two flow parameters have been modified: input power and equivalence ratio. Practically the first leads to different gas mass flow rates and the second to various air quantities. In this way it is possible to define, for every geometric configuration, a lower ignition point, where air quantity is not sufficient to begin the combustion reaction, and an upper quenching point, where the high flow velocity pushes the flame outside the combustion chamber. As for equivalence ratios, it has been decided to focus on lean combustion, neglecting the rich zone because it would lead to the formation of pollutants and low efficiency. Investigating these limits a total number of 322 design points have been measured.

Temperatures of the whole combustion chamber have been recorded. These values have been post processed and the temperatures have been extracted considering the medium line on the combustion chamber. From this array of data, maximum and mean values can be obtained. This technique has been used because a uniform temperature distribution is presumed and values are not affected by geometrical errors, caused by an incorrect spatial discretization.

5.5 Results

In this experimental analysis both fluid and geometrical parameters have been varied to get a better understanding of the performances of the burner. For this reason it is not simple to interpret results regarding the 322 points. All the same, some general trends can be caught. For simplicity, first, every single variable will be analyzed separately, then only the configurations with the 200 mm combustion chamber will be considered and finally results for the 300 mm tube with holes will be presented.

As said, the combustion chamber length has a great influence on quenching phenomena. If the flame does not have sufficient energy to balance heat loss through the combustion chamber the flame will not be able to propagate. On the other hand if flame

stretching is larger than the axial length, part of the flame will be attached to the edge and burn outside the combustion chamber. Between this limit cases, it is necessary to find the correct compromise between high temperature values and uniformity.

Starting from the smaller value, the 100 mm configuration has wide ignition limits. Due to the limited length of the combustion chamber, for several conditions, the flame can be seen partially developing outside the tube, as in Fig. 5.3. Despite this, with high equivalence ratio values the flame stretching determines low temperatures in the first half of the tube, thus leaving a very small emitting area.

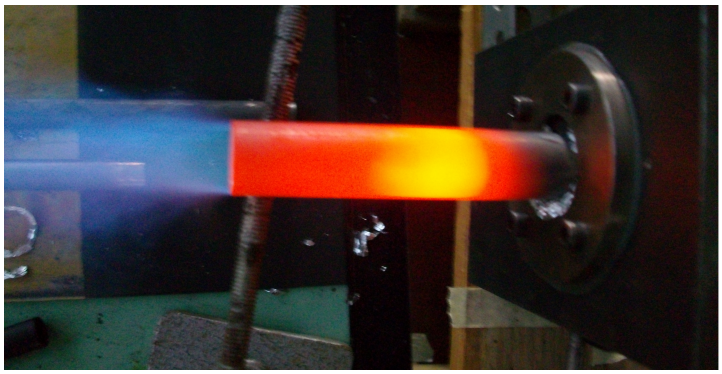

Figure 5.3: 100 mm combustion chamber with external flame and first part with low temperature

On the other hand the 300 millimeter combustion chamber configurations have severe ignition problems. And even in those limited cases combustion is not stable and frequently quenching occurs. The energy of the combustion reaction seems to be smaller than the amount lost due to heat transfer, both radiative and convective, at the external surface of the combustion chamber.

Figure 5.4: 300 mm combustion chamber

The 200 mm combustion chamber has the best results considering the three output parameters. Operating conditions are stable for the different geometric parameters and flow conditions. Temperature values are uniform over the entire length, leading to a high total emissive power value. Results for this type of configuration will be analyzed in detail in the next section.

Considering the inner tube, although the length difference was only 2 millimeters, the behavior of the burner was almost antithetic. In fact, using the 18 millimeter one, it was very difficult to ignite the reaction in all conditions, while the other worked fairly well. It is difficult to understand the reason for this difference, since there are no results from inside the burner. Guessing, the reason can be found in two different aspects: mixing and ignition zone. As said before the inner tube length effects the dimension of the mixing zone inside the burner. The reduction of the volume could lead to an insufficient residence time for the molecules to mix. Another explanation could be found in the change of the flow field leading to the modification of the ignition zone and thus the start of the combustion reaction.

The support tube behavior is completely the opposite. In fact, ignition and stability can be found with all values, so it can be said that this parameter has less influence on combustion dynamics than the others. But among this, it influences overall performances: decreasing the length of the support tube leads to higher mean temperature values.

More precise results can be obtained looking at values of mean and maximum temperature recorded with the IR thermal camera. Graphs and plots have been done using ModeFrontier for its capability to handle a large amount of data and perform a statistical analysis, considering the different design points. A first analysis can be done looking at emitter maximum and mean temperature values, considering the mean line on the emitter. Results are summarized in table 5.2.

	minimum value	mean value	maximum value
Mean temperature	401.3	677.9	837.79
Maximum temperature	603.1	881.6	972.1

Table 5.2: maximum, minimum and mean temperature values

These values do not give much information of the results obtained in the experimental test. A qualitative prospective can be found looking at the related histogram and cumulative function, represented in Fig. 5.5. It can be seen that the distribution differs from a Gaussian with the mean shifted towards high values. In fact, looking at the cumulative probability function, 50% of the points have a maximum temperature above 900 °C. Mean temperature values have a similar distribution but are widely spread and

more uniform, considering the range of 650 °C till 750 °C. 50 % of the design points have a higher temperature than approximately 680 °C.

Maximum and mean temperatures are related, but less than expected considering the two distributions and the correlation factor, defined in Ref. (4), which has a value of 0.705. In fact, in both histograms are highlighted designs with the same maximum temperatures, these are spread in the mean temperature one. This only enforces the idea that peak temperatures are not so important, or even lead to a non-uniform distribution in the axial direction.

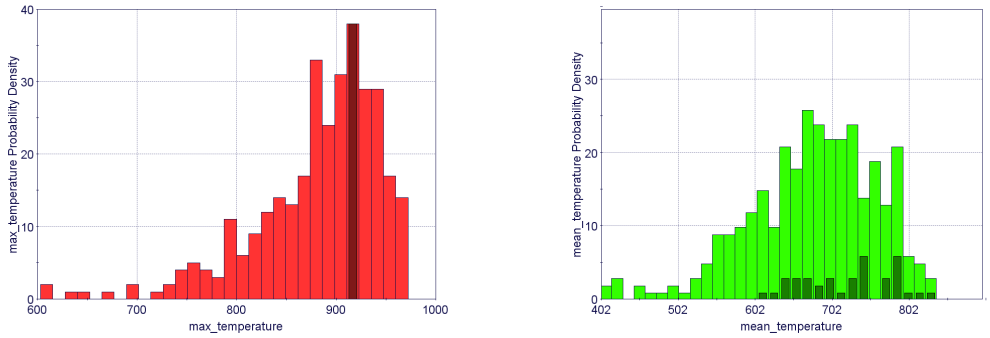

Figure 5.5: Histogram for maximum (left) and mean (right) temperature

5.5.1 200 mm combustion chamber

The combustion tube length is certainly one the most important geometrical parameters of a TPV system because it influences the burner dynamics and the cell electrical output. In fact, the area of the emitter is related to the surface and thus the number of cells. At the moment being, the type of cells and the assembly are unknown, so it is impossible to calculate the electrical output of the stack of thermophotovoltaic cells from the obtained temperature profile.

Thus, considering only burner performances, it can be seen that the intermediate length, corresponding to 200 millimeters, seems to be the best option. In this section results will be analyzed carefully considering relations and trends of the 129 collected points, which correspond to this fixed value of emitter length. From this other 16 points corresponding to an inner tube length of 18 mm have not been considered because of combustion instability.

As done before, ranges for mean and maximum temperature have been summarized in table 5.3. Comparing these values with table 5.1, it can be seen that the maximum

value belongs to this configuration, while the mean temperature is 10 °C lower than in the previous case, on the other hand minimum values are significantly higher now.

	minimum value	mean value	maximum value
Mean temperature	555.1	713.9	826.8
Maximum temperature	701.4	899.4	972.1

Table 5.3: Maximum and mean temperature values

To understand the importance of each variable on mean temperature value correlation factors can be calculated. The degree of the relation is expressed from -1 to 1 indicating the linear association to be direct or opposite in sign. Values are plotted in the correlation matrix chart in Fig. 5.6.

Mean temperature values are mainly affected by equivalence ratio, this partly is due to the wide range of values dictated by ignition limits. But it is also due to combustion dynamics: in fact, higher mass flow rates tend to stretch the flame causing it to exit the combustion chamber and thus lose energy in the external environment. At the same time chemical kinetics are influenced by air mass fraction, which determine flame temperature and products generation. It is interesting to see how power influences emitter temperature: decreasing power leads to lower maximum temperatures and higher mean values, leading the higher efficiencies. Considering only this emitter length, the correlation between the two temperatures has decreased to a value of 0.468 from 0.705, for all configurations. The support tube length effects only the temperature profile in an inverse relation and has more importance than the input value of power.

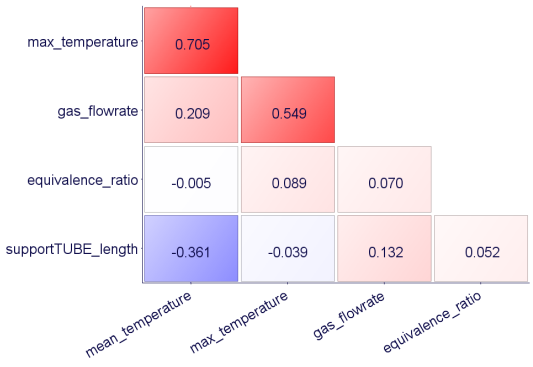

Figure 5.6: Correlation factor chart

In Fig. 5.7 mean temperature is shown as a function of equivalence ratio for different

power values and a fixed support tube length. The represented results reffer to no support tube. The graphs regarding the other configurations have similar trends, so the conclusions can be accepted as valid for all the design points. The higher values are obtained at 3 kW, while 2 kW and 4 kW have similar results at lower values of equivalence ratio, but after 1.6 for the second case performances decrease rapidly. For the maximum power of 5 kW, mean temperature is the lowest of the whole range. Two interesting aspects can be seen considering 2 kW and 3 kW power values. Considering equivalence ratio, in the range between 1.4 and 1.9, mean temperature has a parabolic distribution with a maximum at approximately 1.7.

Temperature for 1.4, 1.76, location corresponding to the maximum and 1.85 are 803.1 °C, 821.8 °C and 801.7 °C respectively. This is positive aspect regarding pollutant formation: in fact, lean combustion decreases the maximum flame temperature and thus the NO_x formation, without compromising the emitter performance. This trend is very different from the adiabatic flame temperature which decreases monotonically with equivalence ratio, this means heat transfer and flame stretching have a dominant role in this range respect to combustion temperature. The other interesting aspect can be found in the very lean region, after a value of 2. The 2 kW configuration has higher temperature respect the 3 kW, because it decreases slower toward the extinction point, at high equivalence ratio values.

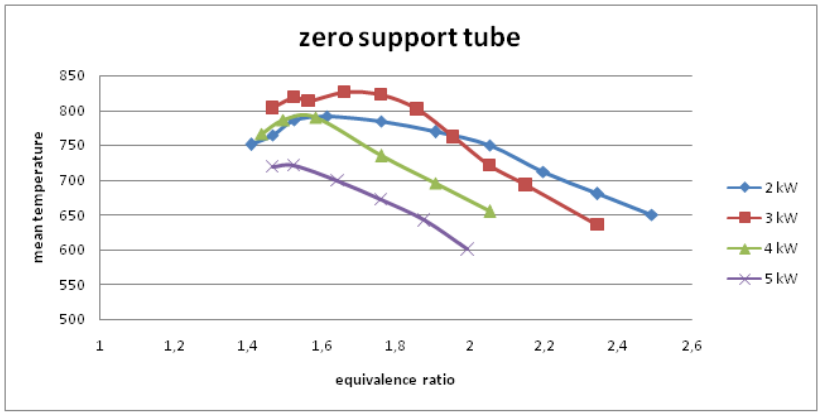

Figure 5.7: Mean temperature as function of equivalence ratio with no support tube at different power values

Mean and maximum values of temperature can only give an idea of the performance of the burner. But, as said previously, uniformity is maybe even more important for the final electrical output of the system. To judge this property the only way is to analyze

the temperature profile on the emitter surface.

Considering the 3 kW value of power and no support tube, the temperature profile on the axis of the emitter can be plotted from the IR images. In Fig. 5.8 four values of equivalence ratio have been taken into account: 1.47 (red), 1.66 (blue), 1.95 (cyan) and 2.35 (green). The lower values have a similar trend: the rise in temperature is very close to the entrance, has a peak at about half the length and then decreases with a smooth slope towards the exit of the combustion chamber. Increasing mass flow rate, the temperature rise is shifted in the axial direction towards the exit, reaching the maximum at 119 millimeters and 169 millimeters, respectively for 1.95 and 2.35 of equivalence ratio values. It is interesting to note that temperatures in all four cases are almost identical at the exit of the chamber, approximatlely 750 °C. This difference is probably due to a slight movement of the thermal camera when taking the images.

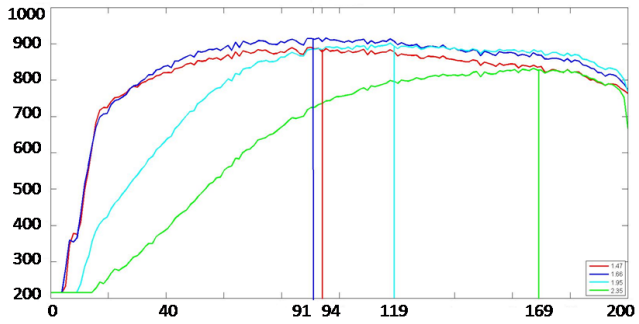

Figure 5.8: Temperature profile in the axial direction for different equivalence ratio

This difference in the first part depends on the flame structure and combustion dynamics. At first insight this behavior can be ascribed to the impinging point of the flame on the walls of the combustion chamber. In fact, increasing mass flow rate the angle of the diverging flow gets smaller, increasing the axial position of that point. But this is not true for this burner, in fact, as it will be analyzed in the next chapter, visualizing the flame shape with the quartz tube, no significant difference can be seen in the sudden expansion region. Then the most likely explanation can be found in phenomena regarding flame stretching and reaction kinetics. The production of heat is spread on a wider surface, with reactions occurring more slowly, thus decreasing temperature values. Not knowing the flow characteristics, temperature distribution or species concentration inside the burner, these considerations represent only a guess of physical explanation of these results. Further analysis will finally clarify what actually occurs inside the mixing zone and the development of the flame inside the combustion chamber.

The last geometrical parameter to analyze is the support tube length. The total length of the 14 mm tube is due to the sum with the inner tube, but it has been seen that this value effects more the combustion dynamics, while the other ignition. In Fig. 5.9 are reported mean temperature values for different power with a fixed equivalence ratio of 1.76. It is clear that with no support tube results are way better than the other cases. It is also interesting to note that the influence of power decreases significantly as values of the support tube increase. As for the previous case the 3 kW configuration performs better than the rest for all values considered.

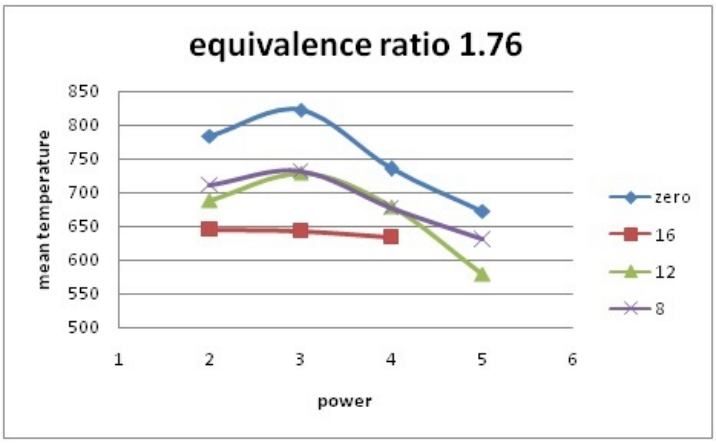

Figure 5.9: Mean temperature as a function of power for different support tube length values

Figure 5.10 shows the IR image consirning the 200 millimeter combustion chamber with a 3 kW input power, 1.7 equivalence ratio and no support tube.

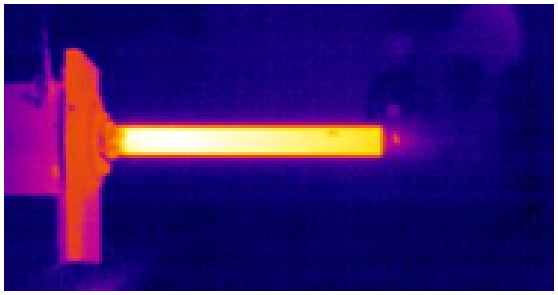

Figure 5.10: IR thermal camera image

5.5.2 300 mm combustion chamber with holes

Having high temperature values is one of the objectives, but at the same time radiation depends on the surface of the emitter. A compromise between these two results has to be found in order to maximize the electrical output. For this reason some efforts to increase the stability of the 300 mm combustion chamber have been tried. Using a central flame holder has not been taken into account because the aim is to get the flame close to the surface wall and not at the centerline of the tube. The device would also block the inner recirculating vortex, which has a positive influence on flame stabilization. Moreover, it has been seen that the flame actually ignites inside the mixing zone so there would be no reason for a flame holder inside the combustion chamber.

Of the different solutions tested, only one proved to work and so has been used with different operating conditions. 4 holes of a millimeter each have been drilled 25 millimeters from the beginning of the combustion chamber. While performing the test, it has been observed that this modification improves combustion stability and enhances emitting performances, as can be seen in Fig. 5.11.

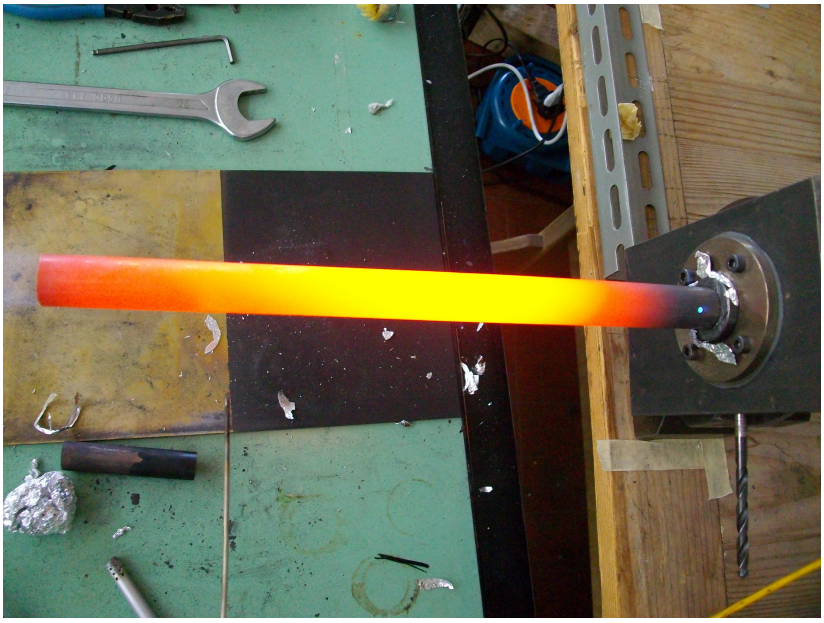

Figure 5.11: The 300 mm combustion chamber with holes

Observing the combustion chamber it is possible to see the flame through the holes. Flow actually exits the holes and no suction can be seen. The height of the flame increases

with power and flow rate. How this changes the velocity profile and shape of the flame is difficult to say.

In Fig. 5.12 temperature profiles in the axial direction for a fixed equivalence ratio of 1.52 and different power values are presented. In this case, performances increase with the increase of power. The higher mean temperatures are reached with 4 kW and 5 kW. Despite this, it can be seen that energy is still not sufficient, since temperature decreases getting to the exit of the combustion chamber. This actually is the opposite situation as recorded in the 200 mm emitter, where higher temperatures were measured for lower power values. This is reasonable since more surface needs more energy to be heated. A very interesting aspect is that there is little difference in the rise of temperature between the four configurations, only with 5 kW, the temperature increases slowly in the first part. Looking at the last 50 mm near the exit of the combustion chamber, the decay in temperature is constant for the different curves, the difference at that point is kept the same till the exit.

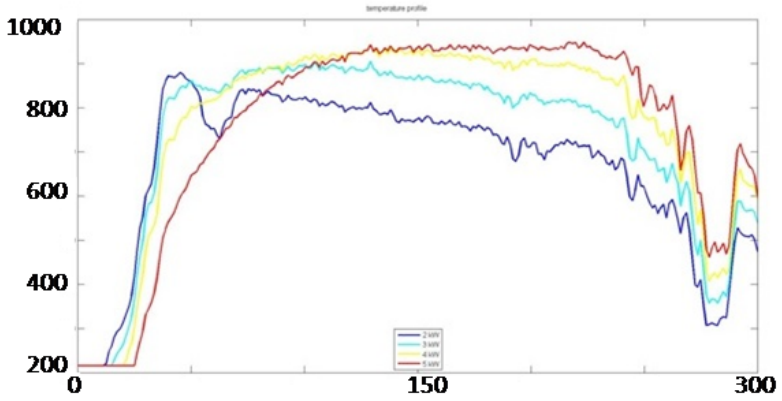

Figure 5.12: temperature profiles on the 300 mm combustion chamber with holes

5.5.3 Quartz combustion chamber

Using a metallic tube gives temperature values on the external surface, which is important for the TPV electrical output, but gives no information on the combustion dynamics inside the burner. Since it is an early stage and many decisions on both geometrical and flow parameters have to be taken, it is very important to understand,

even partially, the development of the flame inside the combustion chamber. For this reason the metallic tube has been replaced with a transparent quartz tube. Measures have been taken keeping the 16 mm inner tube and changing the support tube size, with the values of 16, 12 and 8. The configuration with no support tube has not been tested since it was impossible to fix the quartz tube from the outside because of its fragility.

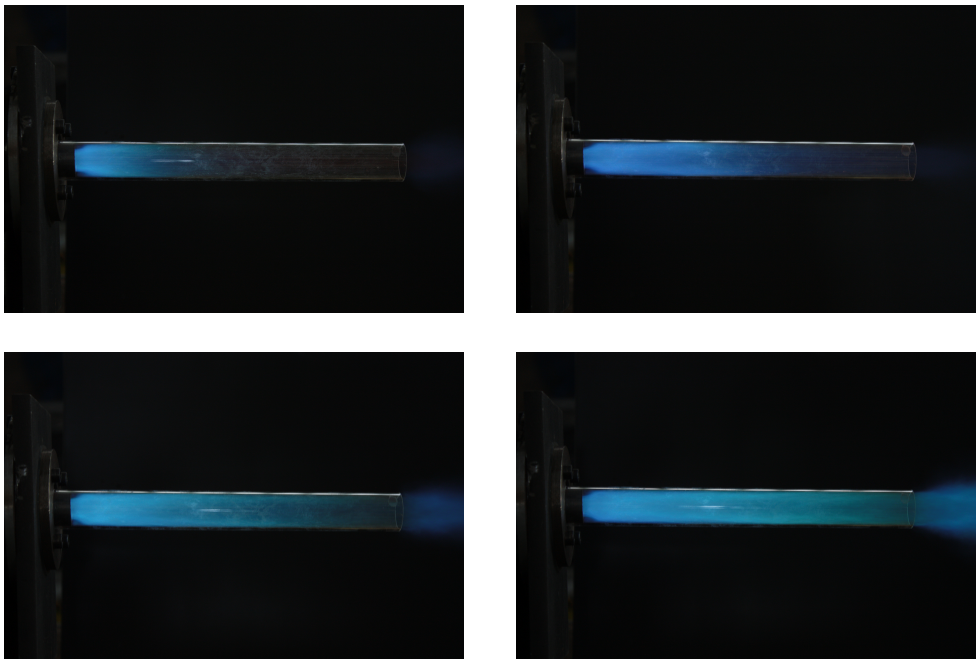

Figure 5.13: Pictures of the flame inside the quartz combustion chamber

Some interesting results have been observed analyzing the pictures taken during the test. Three particular aspects can be seen:

- sudden expansion region
- ignition spot
- flame front stretching

Considering flame dynamics the most important phenomenon observed is that the flame begins inside the mixing chamber. It is not clear where precisely it attaches to the inner tube wall or maybe in correspondence of the hood lid. There has to be somewhere a limited zone where velocity gradients and values match conditions for ignition. The flow entering the inner tube collides with the sharp angle, generating a stagnation zone.

There the combustion reaction could start if the reactants are fully mixed. Ignition limits are very similar to the ones recorded with the metallic tube. This was expected since analyzing the previous results it is clear that geometric measures are the most important variables.

As for the sudden expansion zone the propagation of the flow is, surprisingly, very similar considering different flow rates. This was not expected analyzing at the temperature profiles on the inconel tube, where increasing mass flow rates would shift the peak temperature towards the exit of the combustion chamber. In fact, the flow should get a more jet like shape, decreasing the cone angle at the entrance of the tube and this would move the impinging point in axial direction. This can be explained referring to the nature of the swirling motion inside the burner. Increasing mass flow rate does increase at the same time axial and radial velocity, thus keeping the same ratio between the two components. So the extent of the low temperature zone cannot be due to different attachment lengths.

Another reason could be found in flame stretching and heat release considering the flame front. Increasing flow rate, and therefor velocity, the combustion reactants are spread and concentration of particles decreases. This affects the temperature of exhaust gases and their velocity profile.

5.6 Bibliography

(1) Agema User Manual, *www.agema.com*

(2) www.infrared-thermography.com

(3) S. Basu, Y.-B. Chen, Z.M. Zhang, Microscale radiation in thermophotovoltaic devices - A review, *International Journal of Energy Research*, Vol. 31 (2006), pp. 689 - 716

(4) ModeFrontier User Manual, *www.esteco.com*

6

OPTIMIZATION

Experimental analysis is very useful in determining the real performances of a system, collecting data for simulations and verifying design choices. But at the same time it is time consuming: preparing, setting up and finally obtaining results can take months or more. For this reason it is impossible to perform measures for all the different combinations regarding the different input variables. But on the other hand a small number of measures can bring to incomplete or incorrect results.

A solution to this problem is trying to find relations between input and output variables considering non dimensional parameters. This is not a simple task if dealing with complex phenomena with turbulent flows, combustion and heat transfer, especially if precise data are not available because of incomplete measures.

Another solution is using optimization algorithms to find values for points, which have not been measured during the experiment. In this way it is possible to save time and have detailed data.To complete this task, response surface algorithms (also known as metamodels) can be used. In this chapter some theoretical background will be presented, since in literature it is possible to find detailed information and mathematical explanations as in Refs. (1), (2) and (3). Later the process used to obtain results will be presented considering all the steps taken. Finally results from the optimization will be analyzed.

6.1 Response surface algorithms

The response surface methodology (RSM) is based on algorithms used to determine an approximated function of an output variable concerning the input parameters, as defined in Ref. (1). In practice, known points, determined through numerical or experimental analysis are considered as a mathematical function, without considering the process used in the determination of results. RSM can be divided into two different categories: in-

terpolating, which pass exactly through the database points and approximating, which minimize the extrapolation error on the points.

In order to calculate and judge the accuracy of a RSM metamodel two steps have to be performed:

1. training
2. validation

In the first step the dataset is used by the algorithm to determine parameters and constants of the mathematical function in order to minimize the error between the "real" and the "virtual" values. The second step is performed in order to verify the accuracy of the function using points which do not belong to the training set. If residuals, the errors between the two values, are sufficiently small the RSM can be used for an optimization run, otherwise the number of designs of the training set has to be increased.

This is a very interesting and convenient tool for computationally costly simulations or long experiments. In fact, the virtual calculation using metamodels is very fast, only a few seconds, thus allowing a large number of configurations to be calculated. Coupled with an optimization algorithm it allows to reduce the number of design points to analyze in order to find the best solution as presented in Ref. (1).

As an optimization process there are only a couple of general criterions or suggestions regarding which RSM to use. These regard the complexity of the function to be approximated, the time needed for the calculation or the accuracy requested. At the same time it is very difficult to say a priori which RSM can perform the best prediction of the function. The only way is testing different models and determine which has the best results.

6.2 Strategy

ModeFrontier has been used in all steps of the analysis: creation of the database, generation and validation of the RSM and finally the optimization run. First of all the spreadsheet, in excel format, is uploaded through the "data wizard" available inside the software. In this way all variable properties are uploaded automatically inside the program and a workflow is created, as shown in Fig. 6.1.

The experimental analysis has been explained and commented in the previous chapter, so only a few aspects will be recalled. The first step is the selection of the input variables and objectives. The inner tube length will be kept constant to 16 millimeters. The combustion chamber has a wide range and only three lengths have been investigated. Quenching and heat transfer are very complex and the risk of not getting realistic

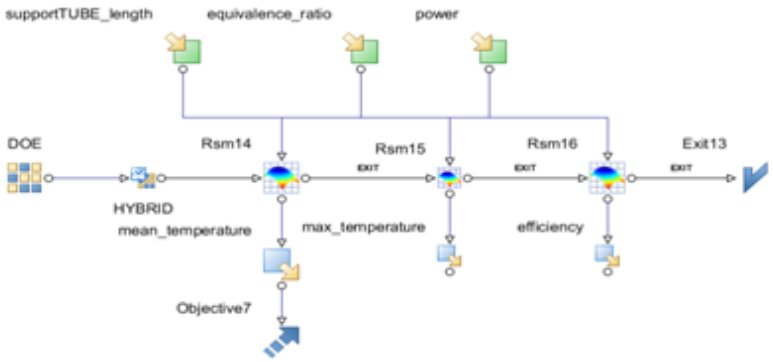

Figure 6.1: ModeFrontier workflow

performances is too high, so even this parameter is kept constant for a value of 200 mm. This leaves the support tube length the only geometric parameter to be varied. As for flow parameters, power values can range from 2 to 5 kW, with a discrete interval of 0.01 between subsequent values. Air to fuel ratio has different ranges, depending on the particular geometric configuration and power considered. Two different strategies can be used: implement inside ModeFrontier a series of constraints in order to exclude unfeasible or try to find common values and eventually delete a few experimental points. The first approach is not very simple since both fluid and geometrical characteristics have to be taken into account at the same time. The second is definitely more simple and straightforward.

Objectives have to be chosen and for every objective a single RSM has to be created. In order to have an insight on the burner performances it has been chosen to evaluate mean temperature as well as efficiency, considered the ratio between the input chemical power and the emitting power. A third output value will be maximum temperature. Even though this variable is related to the average temperature, it will be calculated to have better knowlegde on the temperature distribution. In this way points having best values will be compared to see how these objectives are related to each other.

As explained in the previous section, RSM have to be validated. From the total number of experimental points, half have not been considered because regarding configurations with left out input variable values. This leads to a database of 114 points, from this 15 have been removed and will be used for the validation test, leading to a training dataset of 99 design points. The validation points have been taken for different configurations and operating conditions, in order to have a homogeneous dataset.

The first step is the choice of the correct Response surface, considering residuals from

the training and validation process as well. Since the metamodel has to be trained for a specific output this selection has been done for each objective. The process will be presented theoretically and then results will be explained for each RSM.

6.3 Theory

Inside ModeFrontier several types of RSM are available:

- Polynomial Singular Value Decomposition (PSVD)
- Radial Basis Function (RBF)
- Gaussian Process
- K-Nearest
- Kriging
- Anisitropic Kriging
- Neural Network (NN)
- Evolutionary Design (ED)

Polynomial singular value decomposition (PSVD) is a metamodel based on the minimization of the squares of the error through an elementary polynomial function. Increasing the degree the error is reduced but at the same time the requested number of points of the dataset has to be enhanced, otherwise the problem is undetermined. Considering k the number of parameters and n the degree of the polynomial function, the requested number of training points m can be found with the expression:

$$m = \frac{(k+n)!}{n!k!}$$

Considering three input parameters, the maximum degree is 6 since the minimum number of training points is 84, while for a seventh order polynomial 120 points are needed. In order to have a correct approximation the variables are normalized to obtain values between 0 and 1. Three different cases have been tested considering a first, third and sixth order polynomial. The maximum absolute error decreases from 89 to 45 to 18, respectively, and the absolute minimum error goes from 30 to 9 to 3. In Figs. 6.2 and 6.3 are shown the errors, relative to the mean temperature response surface, in the three cases and the values of the computed coefficients for the first and third order PSVD.

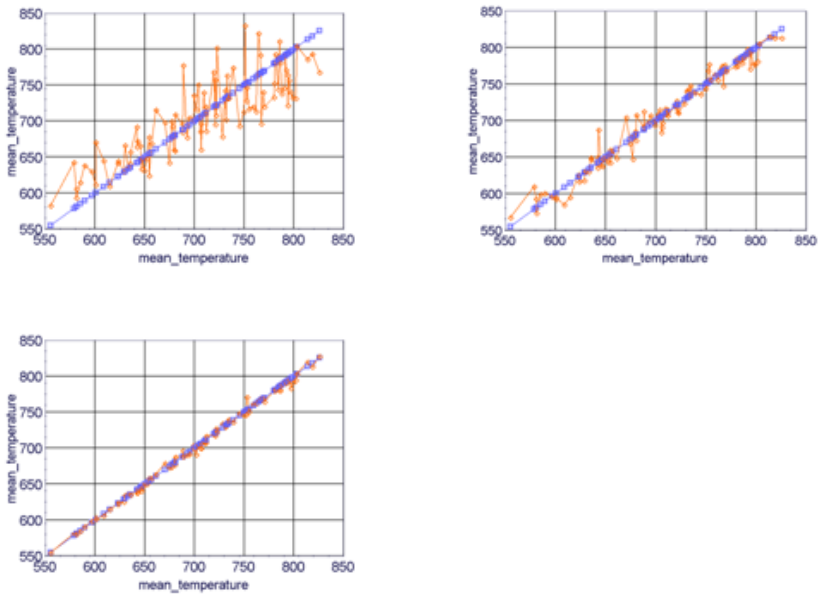

Figure 6.2: Comparison between training dataset and computed values through PSVD, first order (top left), third order (top right) and sixth order (bottom) polynomial

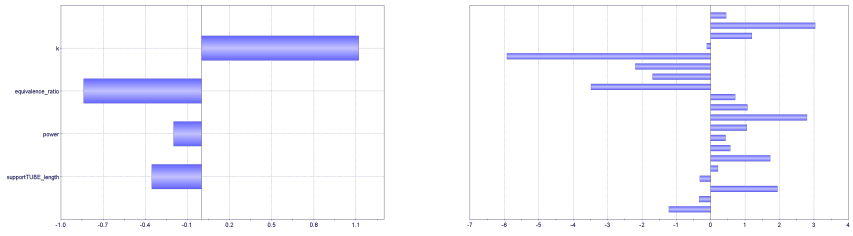

Figure 6.3: Values of the coefficients of the first and third order PSVD metamodel

Shepard K-Nearest is an interpolating metamodel based on probabilistic assumptions, that is the function will pass exactly through the training points. For this reason it is impossible to judge a priori the performance of the response surface. Mathematically, as described in Ref. (4) for the Shepard formulation, the solution is obtained considering a weighted average of different points, where weights are inversely proportional to the distance at which the encountered point is from the calculated one as in Ref. (4):

$$w_i = \sum_{j=1}^{n} \frac{\|x - x_{i,j}\|^{-p}}{\sum_{j=1}^{n} \|x - x_{i,j}\|^{-p}}$$

Where p is an exponential term put to 2 after a series of benchmark tests and n is the number of experimental points. In the K-Nearest version n is replaced by $k < n$, considering only part of the nearest points, by default k is 10 in ModeFrontier.

Kriging is a metamodel which belongs to the family of least mean square methods. The mathematical function uses the covariance function. There are several different variants of this metamodel depending on the type of covariance function, or variogram, used:

- Gaussian
- Matern 5/2, Matern 3/2
- Rational Q 0.5, Rational Q 2
- Exponential

In order to decide which to use, the maximum and mean absolute error, as well as the likelihood have to be analyzed. "The Likelihood of the variogram is the probability that a statistical distribution associated to the variogram parameters could generate the given dataset" is the definition given in Ref. (2). This means the larger this value is, the better the metamodel is fitting the dataset. The best method is associated with the Gaussian distribution.

Anisitropic Kriging is a variation of the method described before. As explained in Ref. (5) in this case different importance is given to each of the input parameters. In this case the Gaussian distribution is used as done previously.

Evolutionary design is an advanced metamodel based on genetic algorithm programming. The main difference with the previous methods is that the form of the regression function is not decided a priori. In fact, primitive arithmetic, elementary, trigonometric and hyperbolic functions are used to generate the output parameter. Increasing the number of considered functions in the database the evaluation and training time will be enhanced. The genetic algorithm searches not just a combination of primitive functions, but also the number of coefficients and respective values for each, minimizing the error with the training dataset. Four different evolutionary design response surface functions have been trained including progressively more complex functions, but results are very similar, so for simplicity the less complex version has been considered.

Neural Network (NN) is an efficient metamodel based on a set of neurons which can be trained to approximate the output function. This kind of algorithm is implemented in order to work as the human brain. In ModeFrontier the initialization function is based on the Nguyer and Widrow approach, the Levenberg - Marquedt back propagation algorithm is implemented to find the minimum of the error function. The sizing of the network, thus the number of hidden layers, in set to automatic as specified in Ref. (6). Figure 6.4 shows relative and absolute residual values considering the mean temperature RSM.

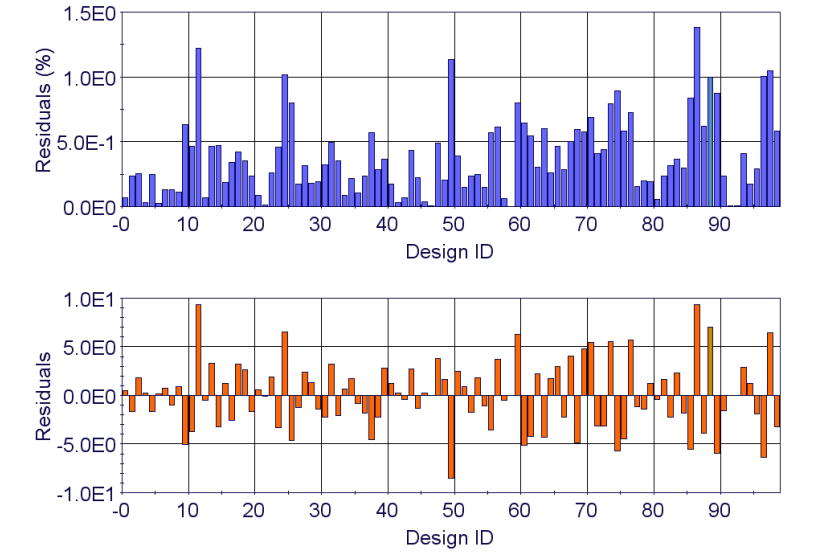

Figure 6.4: Relative (top) and absolute (bottom) residual for the Neural Network metamodel

The Radial basis function method is part of the advanced RSM methods, as explained in Ref. (7). Mathematically, the expression of the interpolant for the response surface is:

$$s(x) = c_j \Phi \left(\|x - x_j\| / \delta \right)$$

Φ is the radial basis function

c_j are coefficients used as free parameters

δ is a fixed scaling parameter.

Changing this last value the shape of the radial function is modified, as can be seen in figure 6.5.

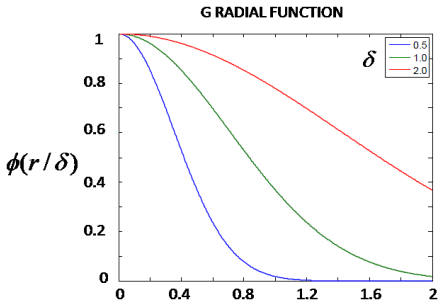

Figure 6.5: Shape of the radial function

In ModeFrontier several functions are available: Duchon's Polyharmonic splines (PS), Hardy's Multiquadratics (MQ), Wendland's Compactly supported (W2), inverse multiquadratic (IMQ) and Gaussians (G). These are summarized in Fig. 6.6 taken from Ref. (6), PD stands for positive definite, the other case is conditionally positive definite (CPD) and d is the number of input variables.

G	$\phi(r) = \exp(-r^2)$	PD
PS	$\phi(r) = \begin{cases} r^3 & d \text{ odd} \\ r^2 \log(r) & d \text{ even} \end{cases}$	$m = (d+1)/2$ $m = d/2$
MQ	$\phi(r) = (1+r^2)^{(1/2)}$	$m = 0$
IMQ	$\phi(r) = (1+r^2)^{(-1/2)}$	PD
W2	$\phi(r) = \begin{cases} (1-r)_+^3 (3r+1) & d = 1 \\ (1-r)_+^4 (4r+1) & d = 2,3 \\ (1-r)_+^5 (5r+1) & d = 4,5 \end{cases}$	PD

Figure 6.6: Mathematical definition of Radial Basis Functions

6.4 Mean temperature RSM

As said before in order to judge the accuracy of a RSM method it is necessary to test it with a set of real points for a validation analysis. The 15 points used have been taken randomly from each different configuration, concerning different values of the input

variables. In Figs. 6.7 and 6.8 the absolute and relative residual values for every point have been plotted considering the different types of response surfaces.

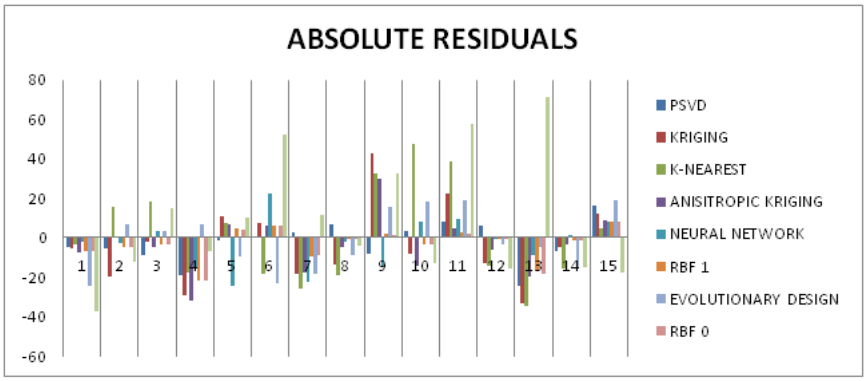

Figure 6.7: Absolute errors considering the validation dataset

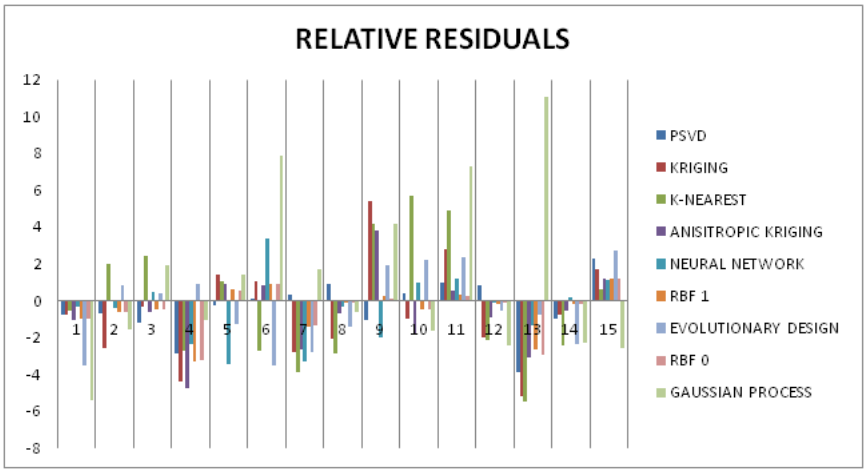

Figure 6.8: Relative errors considering the validation dataset

It is straightforward to see that the Gaussian process method has the biggest errors, in point 13 it actually overpredicts the value of mean temperature while all the other underpredict it. Also Kriging and K-Nearest do not predict results from the experimental analysis with sufficient accuracy. K-Nearest is probably affected by a problem of the flattering of extreme as defined in Ref. (4), in fact points 10 and 11 are maximum points of the function not only in that region but in the whole range. In table 6.1 are summarized values for both errors.

RSM	Maximum residual	Mean residual
PSVD	24.75509	8.140165
KRIGING	42.30402	16.26861
K-NEAREST	47.09506	20.97727
ANISITROPIC KRIGING	31.80313	11.04139
NEURAL NETWORK	24.82719	9.887402
RBF 1	22.01607	6.205711
EVOLUTIONARY DESIGN	24.70565	13.06214
RBF 0	21.75934	6.133145
GAUSSIAN PROCESS	71.48436	24.90787

Table 6.1: maximum and mean residual errors for the different RSM tested

Figure 6.9 shows the mean temperature function comparing real and predicted values, only the most accurate metamodels have been considered. Two radial basis functions have been called 0 and 1 and these respectively use Duchon's Polyharmonic splines and Wendland's Compactly supported models.

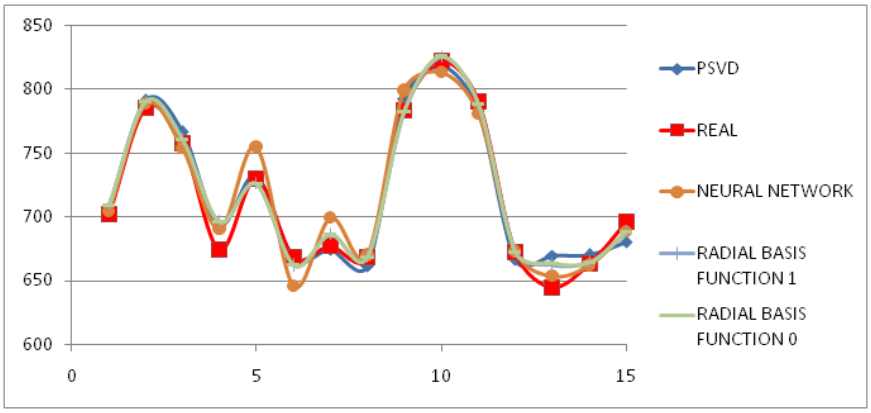

Figure 6.9: The validation dataset

The response surfaces have been trained and validated. Before using a metamodel to perform the optimization of the burner, trends regarding equivalence ratio and input chemical power will be checked. Since the calculation procedure is very fast using RSM both the Radial Basis Function 0 and the Polynomial Singular Value Decomposition will be used, having very close values of accuracy. Results are shown in Fig. 6.10, in which data are referred to 3 kW and no support tube, at different values of equivalence ratio.

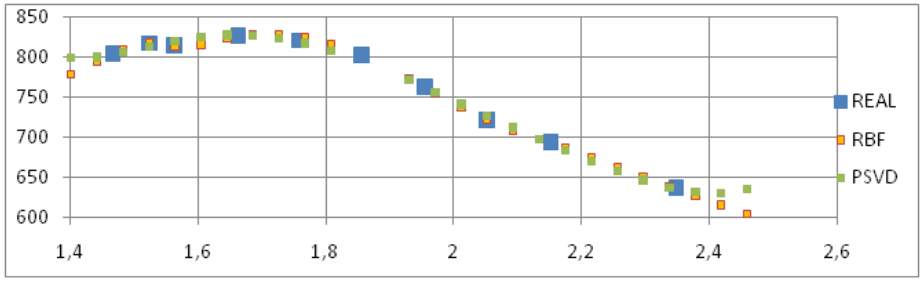

Figure 6.10: Mean temperature value as a function of equivalence ratio for fixed power and support tube length

A second check has been done changing power for a configuration regarding a fixed equivalence ratio of 1.76 and no support tube. During experimental tests and therefor the generation of the metamodels, the range of power has been taken from 2 kW to 5 kW. In this verification the interval has been increased including 1 kW and 6 kW values. No tests have been done with these values, so it is impossible to verify results, but it interesting to see how the two RSM predict mean temperature. PSVD predicts high mean temperature in both cases while RBF low. From experimental analysis and the trend of the function it is possible to say that RBF does not get the right trend for 6 kW. For 1 kW the same conclusion can be drawn, predicted mean temperature of over 1000 $°C$ is over 150 $°C$ higher than the maximum value measured in the experiments, for this reason it seems an unrealistic prediction. On the other hand, values obtained with RBF seem to be in good agreement with the rest of design points, as shown in Fig. 6.11.

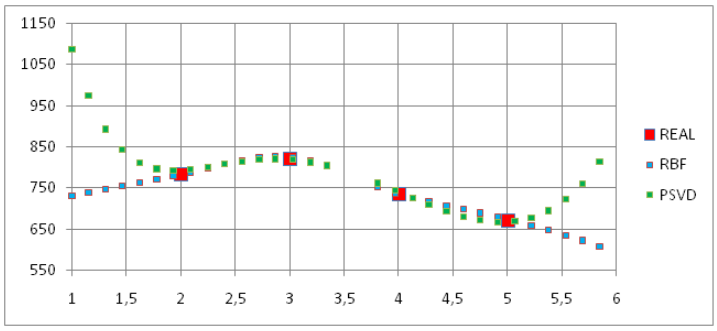

Figure 6.11: Mean temperature as a function of power for fixed values of equivalence ratio and support tube length

6.5 Efficiency and maximum temperature RSM

As said previously a single RSM has to be created for each output variable. The whole procedure done for mean temperature has been repeated for efficiency. In this section only some results will be presented. In Fig. 6.12 the efficiency function is shown for the 15 validation points, while in Table 6.2 maximum and mean errors are presented for the maximum temperature RSM

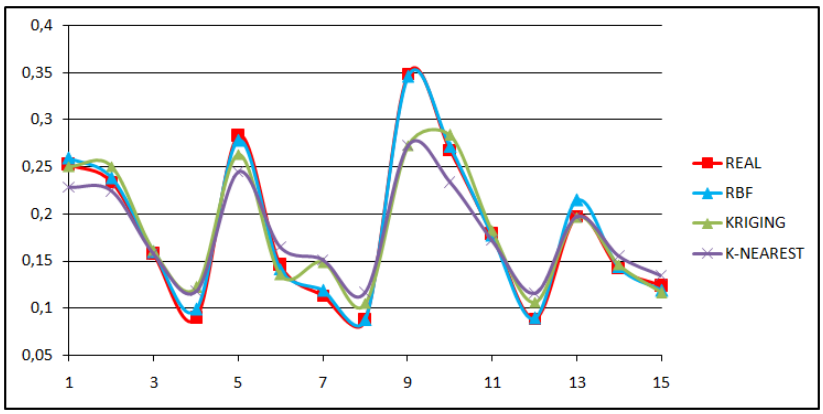

Figure 6.12: Mean temperature as a function of power for fixed values of equivalence ratio and support tube length

RSM	Maximum residual	Mean residual
PSVD	27.33	6.69
KRIGING	32.79	11.83
K-NEAREST	51.59	15.81
ANISITROPIC KRIGING	29.85	9.03
NEURAL NETWORK	49.91	10.38
EVOLUTIONARY DESIGN	16.33	5.82
RBF 0	29.99	8.46

Table 6.2: Maximum and mean residual errors for the different RSM tested for maximum temperature

6.6 Multi-objective Optimization

Now that the response surfaces have been trained and validated in the three cases it is possible to perform an optimization on the burner preformances. The three output variables have been considered objectives in a multi-objective genetic algorithm, which works as an evolution process. Computationally this method is implemented in a repeated loop, starting from an initial population of design points. Performances are evaluated and a selection of the best designs is done. Then a crossover and a mutation of the individuals is done in order to maintain fitness in the solution. Finally the performances of the new generation are performed and a new step starts. In this optimization the MOGA II genetic algorithm available inside ModeFrontier has been used considering a population of 100 designs and 200 generations, for a total number of 20000 estimated points.

For all three output variables the RBF function has been used. Although for maximum temperature PSVD had to minimum error, RBF has been chosen for its stability at the extremes of the interval as seen for mean temperature in Fig. 6.11. In Table 6.3 accuracy for each are summarized.

Output Variable	RSM	Maximum error	Mean error
Efficiency	RBF	0.017 [-]	0.0044 [-]
Maximum Temperature	RBF	30.0 [$°C$]	8.46 [$°C$]
Mean Temperature	RBF	21.75 [$°C$]	6.13 [$°C$]

Table 6.3: accuracy of the metamodels for the optimization run

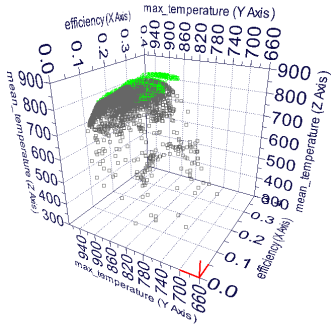

Figure 6.13: Mean temperature as a function of power for fixed values of equivalence ratio and support tube length

Let us now analyze in detail the results obtained in the optimization run. From the 20000 computed designs, 2109 belong to the Pareto frontier. The Pareto frontier is the group of points which have the best performances, considering a non dominant approach of the objectives considered. Two considerations can be done regarding this aspect: the Pareto frontier has a complex shape and a relevant number of points. These characteristics are due to the large number of designs and to the considerations of three objectives. As seen in Fig. 6.13 it is not a simple task to identify a limited region of interest with few designs from which to choose. The points belonging to the front are highlighted in green.

Considering the 2109 points some considerations on the input parameters can be done. Regarding equivalence ratio, values are included in the range from 1.4 to 1.7. As for power, the lower and upper value are respectively 2.2 kW and 3.1 kW. Plotting the obtained results in two dimensional plots, the evolution of the algorithm can be seen.

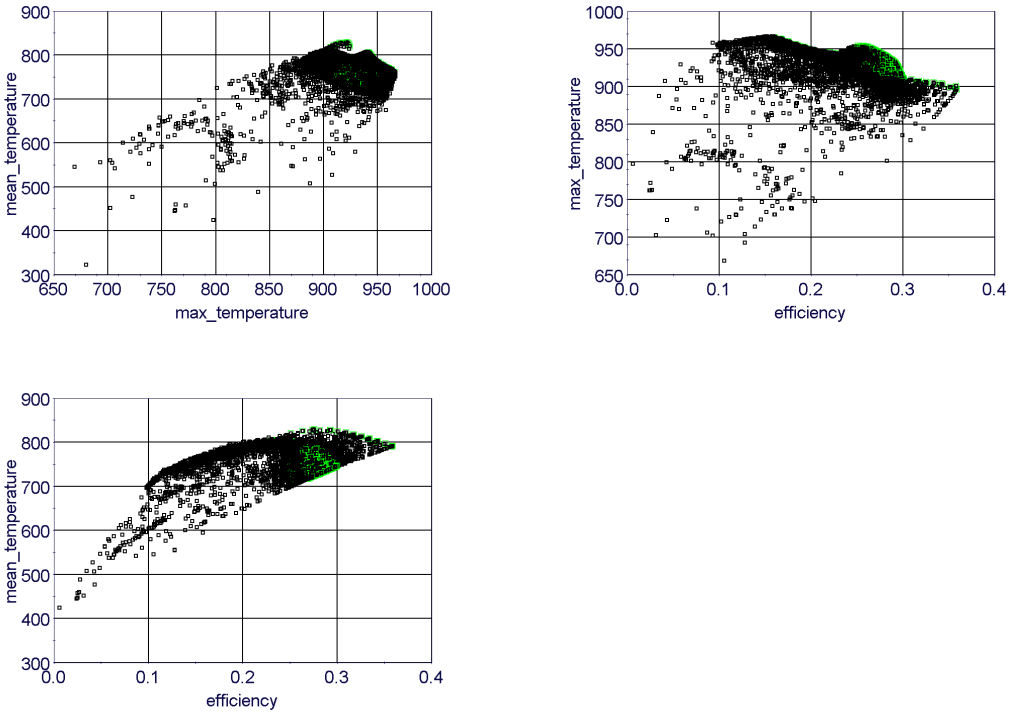

Figure 6.14: Two dimensional plots considering mean temperature, efficiency and maximum temperature

Since, concerning the input variables, mean temperature can be considered the main issue with the development of the burner, it has been chosen to perform a single objective optimization. Two runs have been performed using different algorithms: the SIMPLEX method and the HYBRID algorithm. For a full explanation of the algorithms Ref. (2) can be read. The first does not require the evaluation of derivatives and has been developed from the downhill method for non linear optimization problems of Nelder and Mead. The HYBRID is a combination of the SQP with the genetic algorithm. Results with both did not give an enhancement respect values found with the multi-objective run.

From the designs belonging to the Pareto Frontier one has been chosen as the optimal configuration. Performances and values of the input parameters are summarized in table 6.3. Figure 6.15 shows the temperature profile of the two configurations

Design	Power	E. R.	Inner tube	Mean temp	Max temp	Efficiency
Optimal	3 kW	1.7	0 mm	829 $°C$	921 $°C$	0.257
Starting	2 kW	1.9	8 mm	677 $°C$	799 $°C$	0.22

Table 6.4: starting and optimized burner characteristics

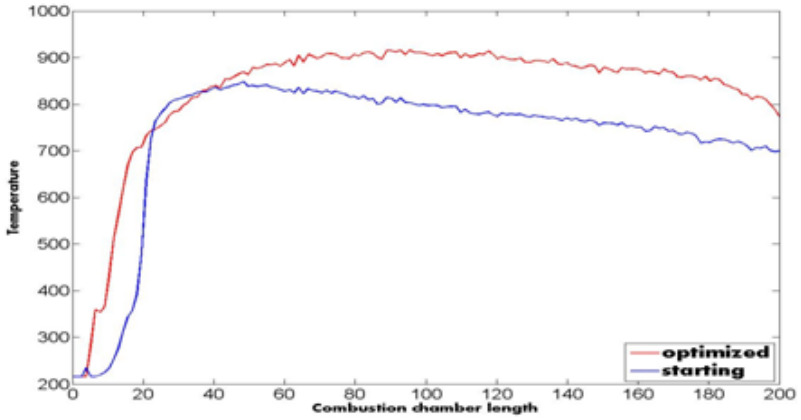

Figure 6.15: Temperature profile of the starting and optimized configuration

6.7 Bibliography

(1) Marco Cavazzuti, Optimization MethodsFrom Theory to Design Scientific and Technological Aspects in Mechanics, *Springerlink* 2013, ISBN: 978-3-642-31186-4 (Print), 978-3-642-31187-1 (Online)

(2) ModeFrontier User Manual, *www.esteco.com*

(3)

(4) Silvia Poles, Alberto Lovison, Esteco technical report 2006 - 004, April 14 2006

(5) Alberto Lovison, Esteco technical report 2007 - 004, December 3, 2007

(6) Enrico Rigoni, Esteco technical report 2007 - 001, April 2, 2007

7

CONCLUSIONS

In this PhD thesis the development and optimization of a gas burner for TPV applications has been carried on. This particular system directly converts energy, obtained through a heat source, into electrical power. Residual heat, still present in the exhaust gases, is then used to generate warm air or hot water for the appliance. Although the energy flux is simple to understand the design of a TPV system is quite a challenging task.

Particularly, regarding the burner it is essential to obtain high and uniform emitter temperature. In this novel design, heat transfer, from the flame and the hot products to the surface of the combustion chamber, is maximized by the swirling flow.

The study has been performed using both numerical and experimental analysis. CFD simulations have been done regarding non reacting flow. Experimental tests have given information regarding flame stability and temperature distribution for different operating conditions and geometrical characteristics of the burner.

Although satisfactory results have been obtained with the first prototype, other configurations will be tested in the future. For this case it is not simple to compare results with other TPV systems, since these are still under development in laboratories and university facilities. Even considering only the burner, the use of different fuels (CH_4, H_2), different types of combustion (premixed, porous medium) and nominal power, from micro devices to several kilowatts, a comparison is very difficult.

As emitter other two tubes have been tested recently: SiC and Allumina. Regarding the first, both mean and maximum temperature are lower than obtained with the inconel tube. This is due to the thickness of the combustion chamber, 5 millimeters, respect to 0.5 millimeters. At the same time uniformity is increased. The Allumina tube has a thickness of 3 millimeters and reaches high temperature. All these results are under analysis and will not be included.

Considering the burner another configuration with a quartz reverse tube is under

analysis in the laboratory. Temperatures are enhanced by more than 150 °C, leading to a uniform temperature of approximately 1050 °C. These tests are not completed yet, so results will not be included in this thesis, but will be published in further papers.

In a few cases emission measures have been taken to judge the performance of the burner. Concerning the major species, CO, CO_2 and NO_x, it is possible to say that values are within law restrictions. In some cases, due to the air excess, results are very incouraging, because these are near the limits for ecologic systems.

Referring to the numerical analysis, CFD simulations with reacting flow have to be carried on. With these results it will be possible to optimize the mixing and ignition zone in order to have a stable and complete combustion. In fact, results of the simulations will be used to generate a response surface to use in the optimization run. These then will be used to buid the final prototype.